United States Department of the Interior

Geological Survey

KAOIKI, HAWAII EARTHQUAKE OF NOVEMBER 16, 1983: A PRELIMINARY COMPILATION OF SEISMOGRAPHIC DATA AT THE HAWAIIAN VOLCANO OBSERVATORY

BY

Robert Y. Koyanagi[1], Elliot T. Endo[2], Wilfred R. Tanigawa[1], Jennifer S. Nakata[1], Alvin H. Tomori[1], and Pauline N. Tamura[1]

[1] U.S. Geological Survey
Hawaiian Volcano Observatory
Hawaii National Park, HI 96718

[2] U.S. Geological Survey
Cascades Volcano Observatory
5400 MacArthur Blvd.
Vancouver, WA 98661

Open-File Report

84-798

INTRODUCTION

The extensive seismographic coverage continuously maintained for over 25 years by the U.S. Geological Survey, Hawaiian Volcano Observatory, presents a unique opportunity to examine the seismic history of the Kaoiki seismic zone, locus of the November 16, 1983 earthquake. This paper is a general description and preliminary compilation of seismic data focussed on this earthquake and its aftershocks. One of the authors, Elliot Endo, is preparing a detailed compilation of these seismic data and other geophysical data pertinent to the tectonic features of the Kaoiki region (E. Endo, oral communication).

Hypocenter determination for earthquakes in this report was based mainly on Klein's earthquake location program HYPOINVERSE (Klein, 1978). Additional refinements in P-delays were included in calculating locations for some of the earthquakes used in first motion analysis.

Kaoiki Earthquake of November 16, 1983

At 06:13:01 H.S.T., November 16, 1983, a 6.6-magnitude earthquake struck Hawaii causing substantial damage in the southern parts of the island of Hawaii (Figure 1). The magnitude determined from teleseismic data compiled by U.S. Geological Survey, National Earthquake Information Service (NEIS), was first placed at 6.7, and then revised to 6.6 after averaging more station readings from the worldwide network. The earthquake was located between the summits of Hawaii's active volcanoes, Mauna Loa and Kilauea, at 19°25.8' N latitude and 155°27.2' W longitude, and near the bottom of the volcanic pile at 12 km depth. A preliminary first-motion analysis from local seismic data indicates a strike-slip mechanism (Figure 2). The faulting was the probable result of stresses within the crust induced by magmatic activity. Inflation of the summit regions of both Mauna Loa and Kilauea apparently causes horizontal compression between the two crustal magma reservoirs. The northeast trending nodal plane with a right lateral strike-slip motion is preferred on the basis of the pattern of ground cracking and aftershock distribution of past events.

Maximum intensity was estimated at VIII to IX (Modified Mercalli) in parts of Kapapala, Volcano, Hawaii Volcanoes National Park, Kau and Puna districts, and Hilo (Figure 3 and Table 1). Structural damage was estimated at about 7 million dollars. A comparison of the intensities as a function of distance to other earthquakes of various magnitude in the western U.S. indicate that the Kaoiki earthquake was relatively low in intensity (Figure 4). Intensities of other damaging earthquakes in Hawaii such as the Honomu earthquake in 1973 and Kalapana earthquake in 1975 were similarly lower than expected on the basis of their instrumental magnitude. From the strong-motion seismograph network operated in Hawaii by the U.S. Geological Survey, Branch of Engineering Seismology and Geology, a maximum ground acceleration of .67 g horizontal was measured at the HVO station located at an epicentral distance of 17 km. Amplitude decreased with increasing distance roughly fitting a logrithmic relation, log d = 1.90-.93 g, where d refers to epicentral distance and g is maximum acceleration (Figure 5).

Aftershocks of the November 16, 1983, Kaoiki Earthquake

By the end of November more than 10,000 earthquakes were detected at seismometers a few kilometers from the aftershock zone. Over 800 of these, ranging in magnitude from about 1.0 to 4.3, were selected for processing by computer for location and magnitude. The epicenters were distributed in several concentrations around the main shock encompassing an area of about 20 x 20 km (Figure 6). The aftershock zone enveloped most of the area between the summit of Mauna Loa and Kilauea. The aftershocks were essentially spread upward and outward from the hypocenter of the 12 km-deep main shock (Figure 7 and 8). Crustal earthquakes at 5 to 12 in depth km occurred extensively beneath the epicentral zone, and the lesser numbers of shallow earthquakes at 2 to 5 km in depth were mainly in the northeastern part of the seismic zone. The hypocentral distribution shows no obvious alignment to offer preference for the selection of the fault plane in the strike-slip solution. It is possible that additional treatment of P-delay and station weighting may indicate a systematic bias in our hypocentral determinations.

Except for the events lost in the coda of the major shock and intrumental failures during the initial three hours of activity, the aftershocks were concentrated at a hypocentral distance of 5-6 km from the main shock (Figure 9). There were very few aftershocks within 5 km and essentially none within a kilometer of the principal shock, presumably the result of a significant drop in stress near the time and place of the major initial rupture. The number of aftershocks peak at 5-6 km away, and decay logrithmically with further increase in distance from the main shock.

The numerical and strain release distribution for aftershocks of magnitude 2.0 and larger were mapped according to the scheme summarized in Figure 10. The earthquakes were subdivided by location in grids of one minute of latitude and longitude (equal squares of about 0.4 km on a side), and mapped in four numerical divisions and three depth divisions in Figure 10A. Magnitudes determined for these earthquakes were translated to strain release by taking the square root of energy using a magnitude-energy relation from Richter (1958), $\text{Log } E = 9.9 + 1.9\ M_L - 0.024\ M_L^2$, where E is energy in ergs, and M_L is local magnitude. Strain release values calculated for individual earthquakes in each map grid were summed and contoured in Figure 10B. The earthquake density and log strain release maps define a complex rupture in the lower crust at 5-15 km depth probably caused by a multi-directional pattern of stresses. The principal shock is surrounded by pockets of high earthquake density and strain release along the outlined parts of the semi-circular aftershock zone. There is a relative gap in the central region and adjacent to the main shock as previously indicated in Figure 9. Isolated concentrations of shallow earthquakes trending southwest and especially north of the zone were apparently secondary sources triggered by the principal event. The northern concentration runs into the northeast rift of Mauna Loa near the site of an intrusion of magma following the eruption of July, 1975, which became the site of a major eruption 4 months after the Kaoiki earthquake.

The distribution of aftershocks in space, depth, and magnitude as a function of time appeared generally random or intermittent (Figures 11, 12, 13). Aftershocks scattered widely across the seismic zone with no apparent spatial alignment to chronological sequence. Focal depths ranged mainly from 2 to 12 km during the initial 4 days of intense activity, and then centered persistently

at about 10 km as shallow aftershocks decreased for the rest of November. The aftershocks processed for location ranged from about 1.0 to 4.3 in magnitude, with intermittent high magnitude aftershocks happening mainly during bursts of activity. The numbers of aftershocks plotted cumulatively against time indicate the highest rate of occurrence during the initial 4 days and a gradual decrease thereafter (Figure 14).

Historic Earthquakes in the Kaoiki Region

The Kaoiki is a region of constantly high seismicity in Hawaii. Several tens of earthquakes are commonly recorded each day by nearby seismic stations of the Observatory's 48-station islandwide network. Since 1962, 8,000 earthquakes of about magnitude 1.5 to 6.6 were processed for location and magnitude. The seismicity of the Kaoiki region relative to other areas of activity beneath Hawaii is illustrated in the location map of earthquakes of magnitude 3.0 or greater from 1962 to 1983 (Figure 15). Besides the recent Kaoiki event, two other earthquakes of damaging intensities have occurred beneath the island in the last decade, one beneath Honomu in 1973 and another near Kalapana in 1975.

In the Kaoiki region, there were 3 earthquakes of magnitude 5.5 to 6.6 that generated significant aftershock activity (Figure 16). These events were epicentrally separated about 3 km apart in a NE to SW alignment within the seismic zone, and ranged in depths from 8 to 12 km. Time separation for the events were 12 and 9 years. The extent of aftershock activity is generally dependent on the magnitude of the principal shock, and a logrithmic correlation of the number of aftershocks and magnitude of the principal shock in the Kaoiki is shown in Figure 17. The magnitude of the largest aftershock tends to be higher for large principal shocks. There is no apparent increase of earthquakes in the days before the major earthquakes.

Precursors

In an effort to search for precursors to the recent Kaoiki earthquake, the seismic parameters of strain release, number of earthquakes, and magnitude-frequency are summarized as a function of time in Figure 18. There were no conspicuous short term changes in seismicity to corroborate the radon anomaly detected by the University of Hawaii near the edge of the aftershock zone a few months before the earthquake (Don Thomas, oral communication). On a longer time base major bursts of strain release occurred at about 10-year intervals. Following major aftershock sequences the earthquakes decreased to low rates for several years. About 6 years prior to the major earthquakes in 1974 and 1983 small shocks increased to relatively high rates, and then decreased slightly about 3 years prior to the events. The magnitude-frequency parameter b peaked during the high rate of small earthquakes and subsequently decreased for several years prior to the major events. The b-value for the aftershocks from the November 16 earthquake was low (0.7) and characteristic of tectonic events.

A seismic parameter using the earthquake coda form was also examined for precursory changes but no strong indications were found. The results strongly indicate the need for a more detailed search, and for future reference the procedure used for data reduction and the preliminary results are described in Appendix A.

First Motion Data

A comprehensive compilation of first motion data for earthquakes beneath the southeast flank of Mauna Loa and adjacent regions of Kilauea from 1959 to 1982 was prepared by Endo and others (1984). From this catalogue, about ninety percent of the events with well-constrained solutions for focal mechanism were chosen and mapped in three depth separations, 0-5 km, 5-15 km, and 15-30 km (Figure 19). The large number of samples at 5-15 km depth were plotted separately on 3 maps (Figures 19b, c, d) with the events divided according to location to minimize obscurity introduced by superimposed events in the highly concentrated parts. The alignment pattern of nodal planes for crustal earthquakes at depths less than 16 kilometers from the collection of strike-slip and dip-slip mechanisms indicate a northeast-southwest trending fault system between Mauna Loa and Kilauea. The combination of strike-slip and dip-slip solutions in the major seismic cluster between the summit areas of Kilauea and Mauna Loa imply a complex tectonic region developed by compressional and tensional local stresses. These stresses are presumably induced by the expansion and contraction of the shallow magma storage systems in the two active volcanic centers. The increasing dip-slip pattern along the southwestern increment of the seismic zone suggests decreasing effect of tension and buttressing from Kilauea, and the dominant influence of SW rift dilation and seaward displacement of the unbuttressed south flank of Mauna Loa.

Comparison of Large Earthquakes in Hawaii

Parameters of damaging earthquakes in Hawaii since 1962 are summarized in Table 1. The frequency of aftershocks and intensity of structural damage from these events followed the generally expected relation to earthquake magnitude, depth, and mechanism. The aftershock activity fitting a logrithmic decay pattern and varying in decay rate for 3 damaging earthquakes from different structural regimes is shown in Figure 20. Aftershocks were fewer and decay rate higher for the deep Honomu earthquake in 1973. Damage and felt reports suggested a lower attenuation rate of intensity for the deep earthquake than for the shallower crustal earthquakes. In contrast, the massive horizontal, seaward slippage of the crust enhanced by magmatic loading, and the high magnitude of the Kalapana earthquake in 1975 apparently contributed to the generation of a local tsunami and the notably sustained aftershock activity. Damaging seismic energy mainly propagated seaward and away from the main cultural centers of the island. The 1983 Kaoiki earthquake that occurred further inland with a strike-slip mechanism caused more local damage than the higher magnitude Kalapana earthquake.

Appendix A: Procedure for Preliminary Determination of Earthquake Coda Decay Rate

Seismograms of selected Kaoiki earthquakes from 1980 to 1983 were examined for variations in their coda decay rate that may result from stress changes before and after a significantly large earthquake. A preliminary inspection was made to test the feasibility of using digitized seismograms collected at HVO to resolve systematic changes in the decay rate of the earthquake signal as a function of time. Samples of Kaoiki earthquakes located at 19°24' to 19°28'N latitude, 155°25' to 155°29'W longitude, and depths from 8 to 15 km, essentially within a 7 x 7 x 7 km volume centered on the November 16, 1983 earthquake hypocenter were selected for the analysis. Stations AIN (3-component) and DES (single component vertical) were used to examine the seismic coda because of their epicentrally close locations to the earthquake and operational continuity for more than ten years (Tanigawa, and others, 1983). Also these stations are currently recorded in different formats, and for this preliminary inspection digitized tape records available since 1980 were used. Sample selections were restricted to earthquakes of $M < 1.5$ because of signal saturation and clipping of the larger events. For the data reduction, 12 x 18 cm hard copies of the digitized seismograms from stations AIN, AINE, AINN, and DES were prepared (Figure A1). The seismogram sections included 36 seconds of record at 0.5 cm per second starting from about 5 seconds before the P-wave onset and up to 31 seconds of the earthquake coda. Peak-to-trough amplitude was systematically read at 1-second intervals from the calculated origin time to the end of the record section. The average of 3 to 4 amplitude peaks for each second interval was taken as the recorded measure.

A clear mylar template gridded at 1-second intervals for the abscissa and 5-mm intervals for the ordinate was prepared and used as an aid to read the times and amplitudes. In our analysis of the coda decay rate, we selected the portion of the signal following the S-wave onset, not obscured by signal saturation and clipping level, to the time when the amplitude decay rate decreased to a fluctuating pattern from effects of wave scattering. The logrithmic decrease in amplitude as a function of time was represented by $\log A = x - yt$; where A is amplitude in mm, t is time in seconds following the origin time of the earthquake, and x and y are constants with y representing the decay slope (Figure A2). Seismograms from 42 Kaoiki earthquakes from 1980 to 1983 were reduced, and their derived decay slope (y-value) were plotted as a function of time (Figure A3). In general the decay slope is lower than average after the earthquake and during the aftershock activity. More samples and more source volume constraints need to be applied for a better statistical treatment of the data, and to reduce the fluctuations due to seismic path effects.

Acknowledgement

Much of the data compilation was made with the support of other staff members and seasonal workers at HVO. The authors are particularly grateful for the enthusiatic assistance provided by their summer colleagues Sandra K. L. Zane and Joan M. Yoshioka. Jim Griggs and Maurice Sako furnished photography and drafting needs in the preparation of our figures. Dorothy Footer provided the typing needs to finalize the manuscript. Thanks to our technical reviewers, Jane Buchanan-Banks, Thomas Wright, Patrick Muffler, and Reggie Okamura for their many important comments and guidance.

References

Endo E. T., Crosson, R. S., Koyanagi, R. Y., and Nakata, J. S., 1984, A catalogue of earthquake focal mechanisms for the southeast flank of Mauna Loa, 1959 - 1982: In review of U.S. Geological Survey Open-File Report 84-

Klein F. W., 1978, Hypocenter location program HYPOINVERSE, Part 1: Users guide to versions 1, 2, 3, and 4: U.S. Geological Survey Open-File Report 78-694.

Richter, C. F., 1958, Elementary Seismology: San Francisco, California, W. H. Freeman and Co., p. 359.

Tanigawa, W. R., Nakata, J. S., and Tomori, A. H., 1983, Hawaiian Volcano Observatory Summary 82, seismic data, January to December, 1982: U.S. Geological Survey Preliminary Report.

Figure 1. Location of the 6.6-magnitude Kaoiki earthquake and aftershocks during the initial 10 hours of activity. Local seismic data indicate strike-slip faulting with and east-west orientation of the pressure axis, and a north-south orientation of the tension axis. Darkened circles represent seismic stations on Hawaii that continuously telemeter signals to the U.S.G.S. Hawaiian Volcano Observatory at the summit of Kilauea.

Figure 2. Preliminary first motion analysis of the November 16, 1983 Kaoiki earthquake using local seismic data from the HVO seismic network and plotted on a lower hemisphere projection (prepared by E. Endo). The open circles represent down first motions and solid circles represent up first motions. The direction of maximum and minimum stress are indicated by the T and P, respectively. The preferred fault mechanism based on historic seismic data and pattern of ground cracking is right-lateral strike slip along the northeast trending nodal plane.

Figure 3. Intensity contour map prepared from damage and felt reports from residents compiled by Hawaii County Civil Defense Agency. Intensity is based on the Modified Mercalli Scale.

Figure 4. Approximation of intensity as a function of epicentral distance for the November 16 Kaoiki earthquake and other earthquakes of various magnitude from the western United States.

Figure 5. Maximum acceleration versus distance for the 6.6-magnitude Kaoiki earthquake from records of the U.S. Geological Survey, Hawaii network of strong-motion seismographs. The acceleration data was collected and provided by Arnold V. Acosta and Richard P. Maley of the U.S. Geological Survey.

Figure 6. Earthquake locations in four depth categories between Mauna Loa and Kilauea outlining the Kaoiki aftershock region in November. A-A' and B-B' are reference lines to section plots in Figures 7 and 8, respectively. Symbols for depth and symbol sizes for magnitude are as in Figure 1.

Figure 7. Kaoiki earthquakes in November viewed along a depth section normal to the plane centered on line A-A' in Figure 6.

Figure 8. Kaoiki earthquakes in November viewed along a depth section normal to the plane centered on line B-B' in Figure 6.

Figure 9. Number of aftershocks plotted as a function of distance from the principal shock on November 16. Included were aftershocks during the initial 8 days of activity and at M>1.3.

Figure 10. Earthquake density (column A, left) and seismic strain release (column B, right) maps in 3 depth categories for Kaoiki earthquakes during November 16 to December 31, 1983. Data included earthquakes of 2.0 magnitude or larger located within 19° 15' to 19° 35' latitude and 155° 15' to 155° 40' longitude.

Figure 11. Space-time diagram of earthquakes in the Kaoiki aftershock region within 19° 18.0' to 19° 33.5'N latitude and 155° 18.3' to 155° 32.5'W longitude. The earthquakes in the second half of November are plotted along the line A-A' in Figure 6. Symbols for depth and symbol sizes for magnitude are as in Figure 1.

Figure 12. Depth-time plot of earthquakes in the Kaoiki aftershock region within the map coordinates 19° 18.0 to 19° 33.5'N latitude and 155° 18.3' to 155° 32.5'W longitude. Symbols for depth and symbol sizes for magnitude are as in Figure 1.

Figure 13. Magnitude-time plot of earthquakes in the Kaoiki aftershock region within the map coordinates 19° 18.0' to 19° 33.5'N latitude and 155° 18.3' to 155° 32.5'W longitude. Symbols for depth and symbol sizes for magnitude are as in Figure 1.

Figure 14. Cumulative number of earthquakes of magnitude about 1.3 or greater beneath Hawaii in November.

Figure 15. Location of eathquakes of magnitude 3.0 or larger in the region beneath the island of Hawaii from 1 January, 1962 to 30 November, 1983.

Figure 16. Location of earthquakes of magnitude 3.0 or larger in the Kaoiki region from 1 January, 1962 to 30 November, 1983.

Figure 17. Number of small earthquakes of magnitude 1.5 or more within 5 days before (x), and within 5 days after (0) principal shocks of magnitude greater than 3.0 in the Kaoiki region. The dashed line is the averaged relation between the number of aftershocks and magnitude of the main shocks. Magnitude of the largest aftershock within 5 days following each of the respective principal shocks is shown in the plot to the right. Samples include Kaoiki earthquakes from 1962 to 1983.

Figure 18. Cumulative number of Kaoiki earthquakes of magnitude about 1.5 or greater from January 1, 1962 to November 15, 1983, and cumulative strain release from earthquakes of magnitude 4.0 or greater from January 1, 1955 to November 30, 1983 (lower plot). Strain release was plotted as the square root of energy using Richter's energy-magnitude relation Log $E = 9.9 + 1.9M_L - 0.024M_L^2$. B-values, the magnitude-frequency parameter calculated from Kaoiki earthquakes of magnitude 1.5 or greater plotted as a function of time from January 1, 1962 to October 31, 1983 (higher plot). Samples were taken at 2-year increments with overlapping consecutive years. Value for November, 1983 was calculated and plotted separately.

Figure 19a. Focal mechanisms from lower hemisphere projections for southeast Mauna Loa earthquakes 0-5 km in depth and from 1959 to 1982 in time (after Endo, 1984). Compressional field is black and dilatational area is white.

Figure 19b. Focal mechanism from lower hemisphere projections for Mauna Loa earthquakes 5 to 15 km in depth and from 1959 to 1982 in time (after Endo, 1984). Compressional field is black and dilatational area is white.

Figure 19c. Focal mechanism from lower hemisphere projections for Mauna Loa earthquakes 5 to 15 km in depth and from 1959 to 1982 in time (after Endo, 1984). Compressional field is black and dilatational area is white.

Figure 19d. Focal mechanism from lower hemisphere projections for Mauna Loa earthquakes 5 to 15 km in depth and from 1959 to 1982 in time (after Endo, 1984). Compressional field is black and dilatational area is white.

Figure 19e. Focal mechanism from lower hemisphere projections for Mauna Loa earthquakes 15 to 30 km in depth and from 1959 to 1982 in time (after Endo, 1984). Compressional field is black and dilatational area is white.

Figure 20. Aftershock decay rate for 3 large earthquakes in Hawaii. The rates were approximated from the daily number of magnitude 1.5 or larger aftershocks plotted logrithmically as a function of time for the initial 50 days of activity.

Figure A1. Digitized seismogram of a 1.6-magnitude and 9.4 km deep Kaoiki earthquake on March 20, 1980 at station AIN. Station-to-epicenter distance was 3 km. The dots placed at 02:12:11 mark the calculated origin time of the earthquake to the nearest second. The portion of the seismogram extending from 6 to 17 seconds after origin time as indicated by the horizontal arrow was used to determine the signal decay rate.

Figure A2. Amplitude plotted logrithmically as a function of time. Amplitude readings 6 to 17 seconds after the earthquake origin time were plotted as circled dots and applied in determining the signal decay rate (value for y).

Figure A3. Coda decay slope as a function of time for selected small Kaoiki earthquakes before and after the major Kaoiki earthquake on November 16.

Table 1. Seismic parameters of damaging earthquakes and their aftershocks in Hawaii from 1962 to 1983.

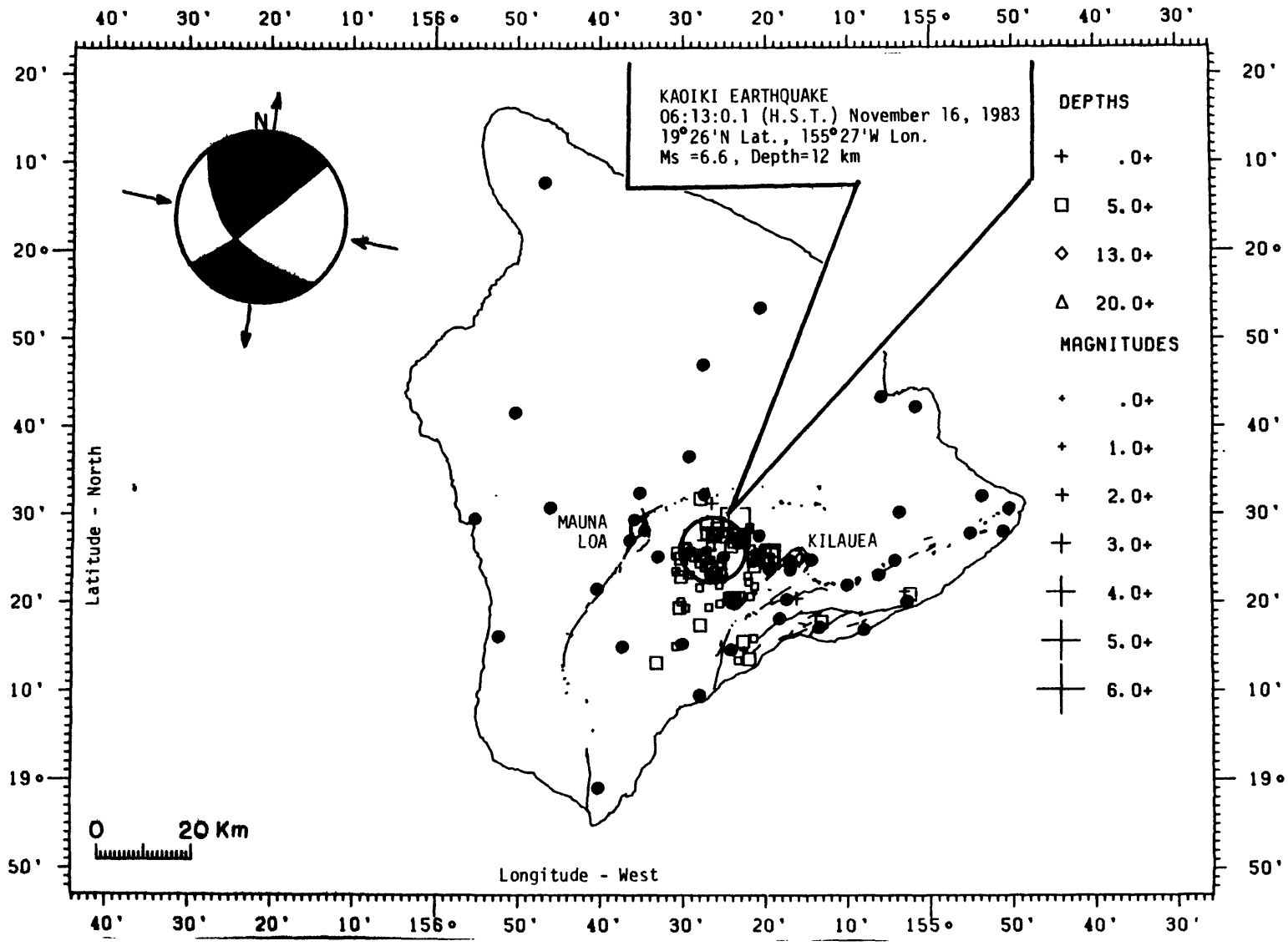

Figure 1. Location of the 6.6-magnitude Kaoiki earthquake and aftershocks during the initial 10 hours of activity. Local seismic data indicate strike-slip faulting with an east-west orientation of the pressure axis, and a north-south orientation of the tension axis. Darkened circles represent seismic stations on Hawaii that continuously telemeter signals to the U.S.G.S. Hawaiian Volcano Observatory at the summit of Kilauea.

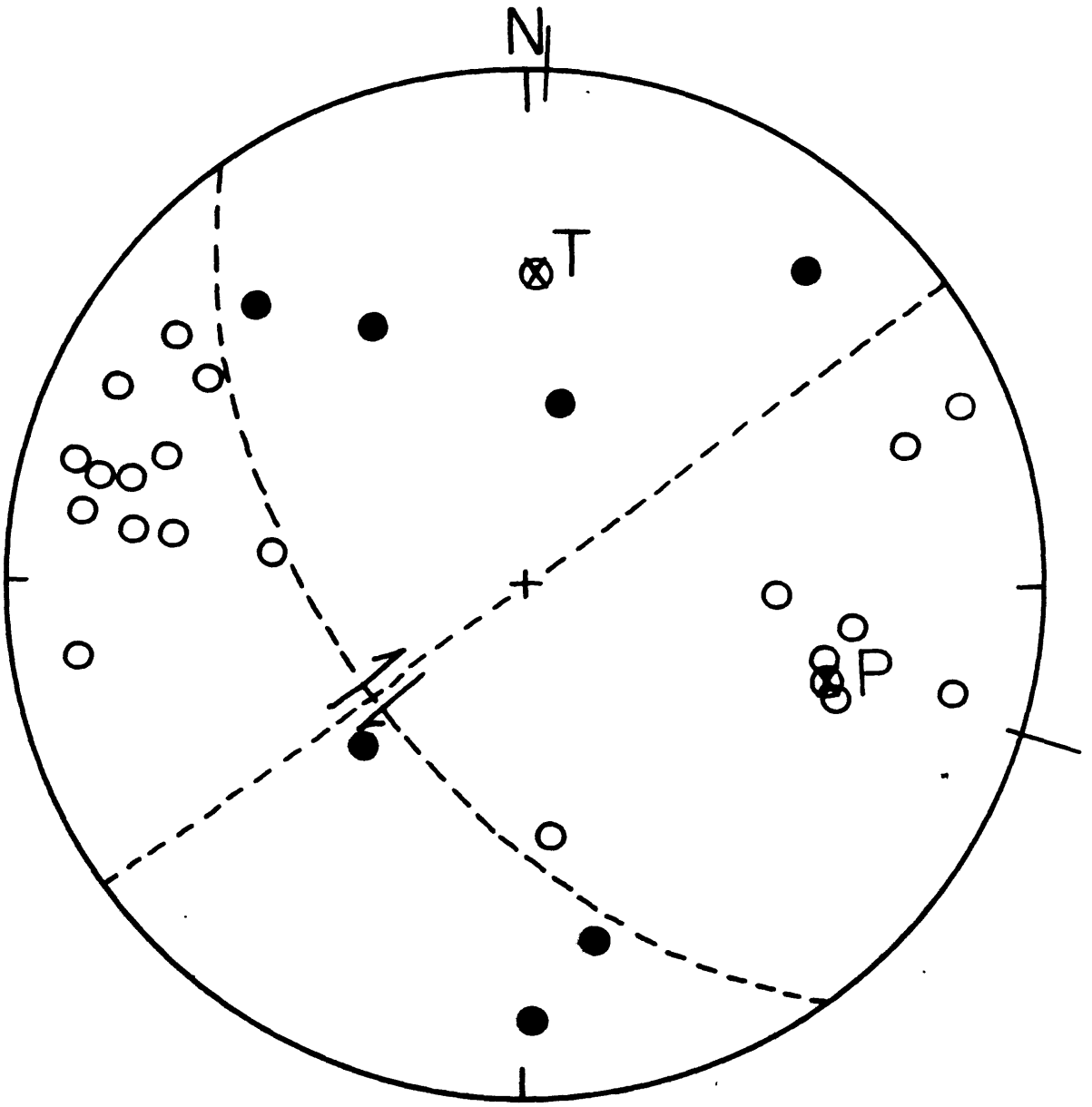

Figure 2. Preliminary first motion analysis of the November 16, 1983 Kaoiki earthquake using local seismic data from the HVO seismic network and plotted on a lower hemisphere projection (prepared by E. Endo). The open circles represent down first motions and solid circles represent up first motions. The direction of maximum and minimum stress are indicated by the T and P, respectively. The preferred fault mechanism based on historic seismic data and pattern of ground cracking is right-lateral strike slip along the northeast trending nodal plane.

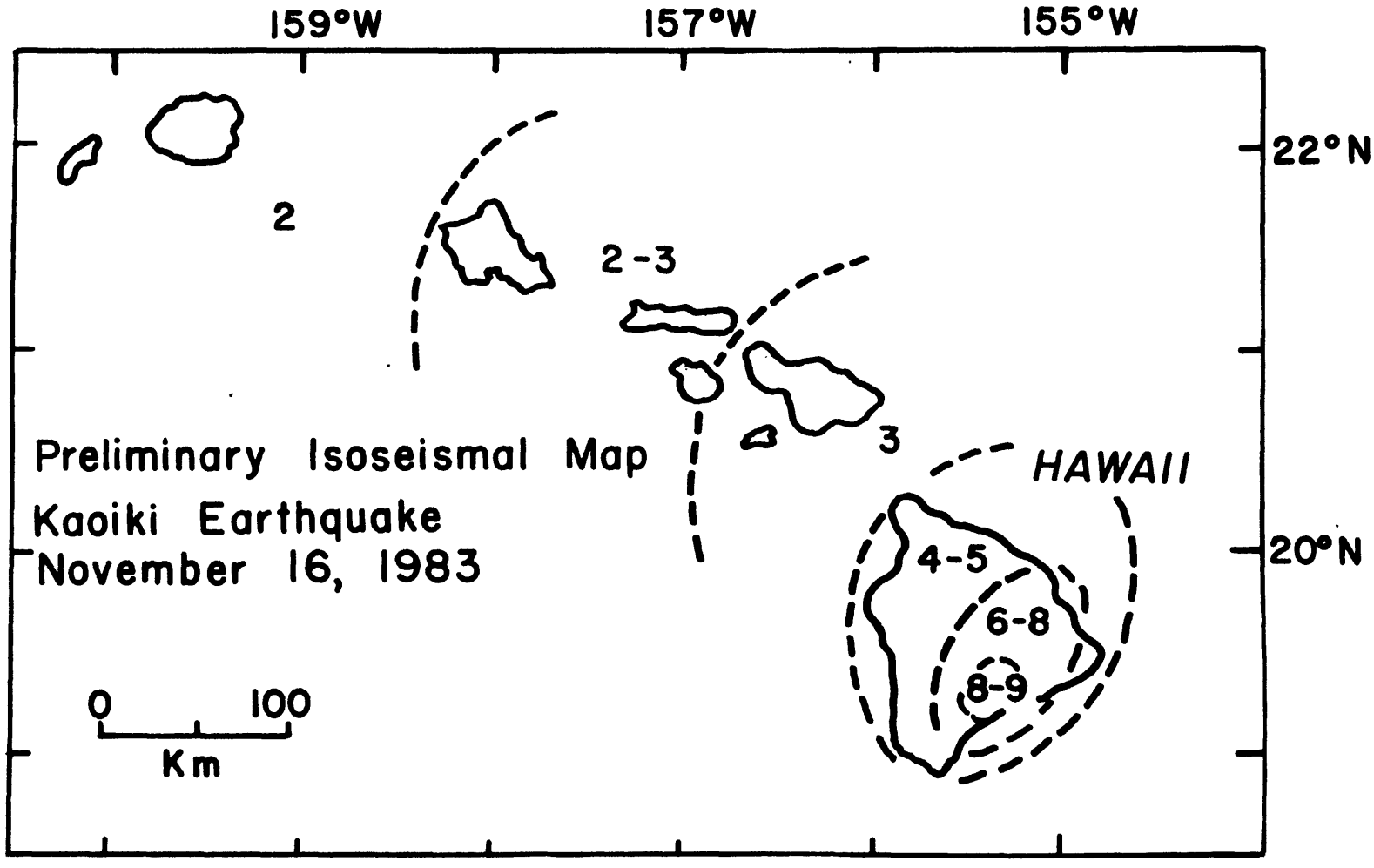

Figure 3. Intensity contour map prepared from damage and felt reports from residents compiled by Hawaii County Civil Defense Agency. Intensity is based on the Modified Mercalli Scale.

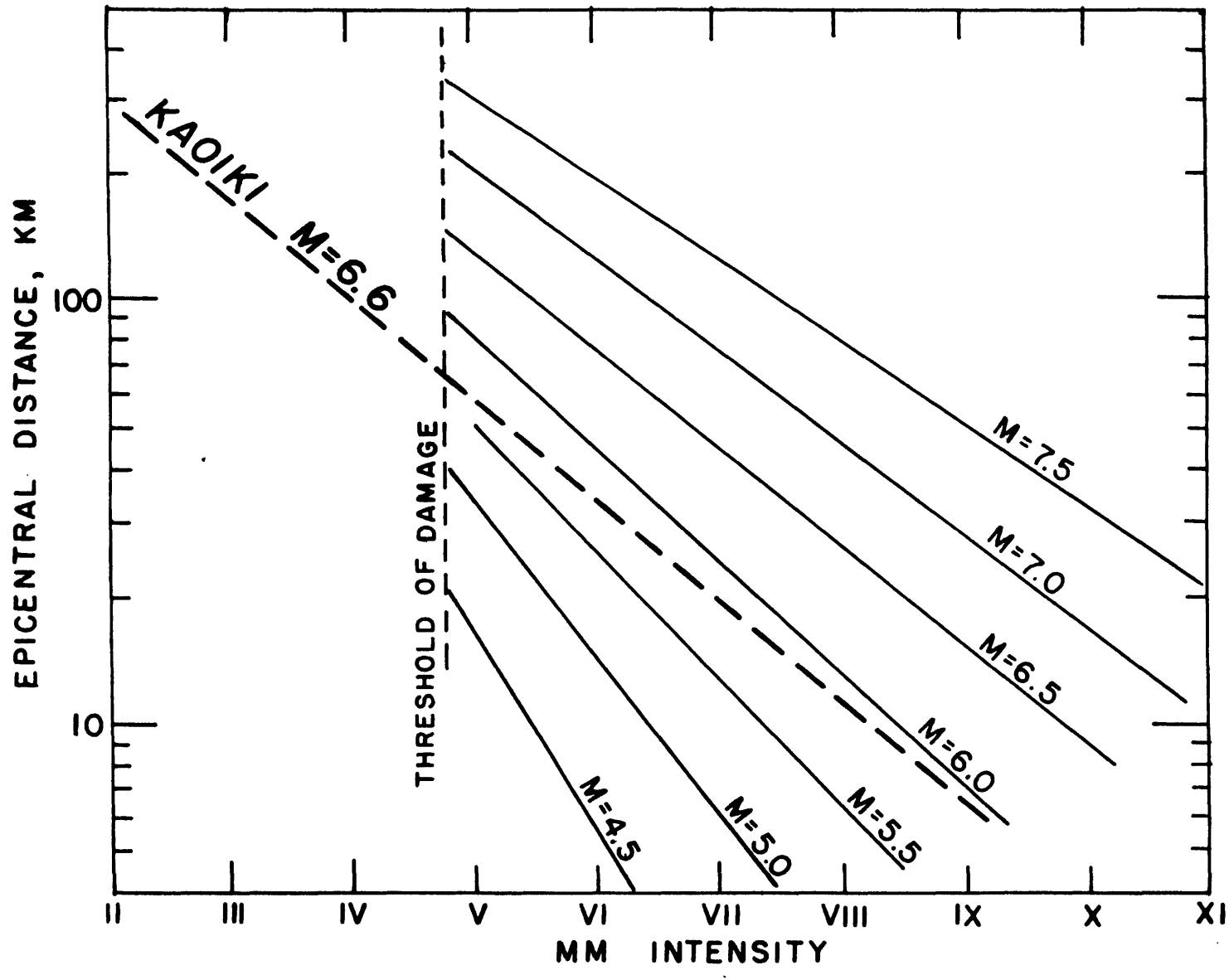

Figure 4. Approximation of intensity as a function of epicentral distance for the November 16 Kaoiki earthquake and other earthquakes of various magnitude from the western United States.

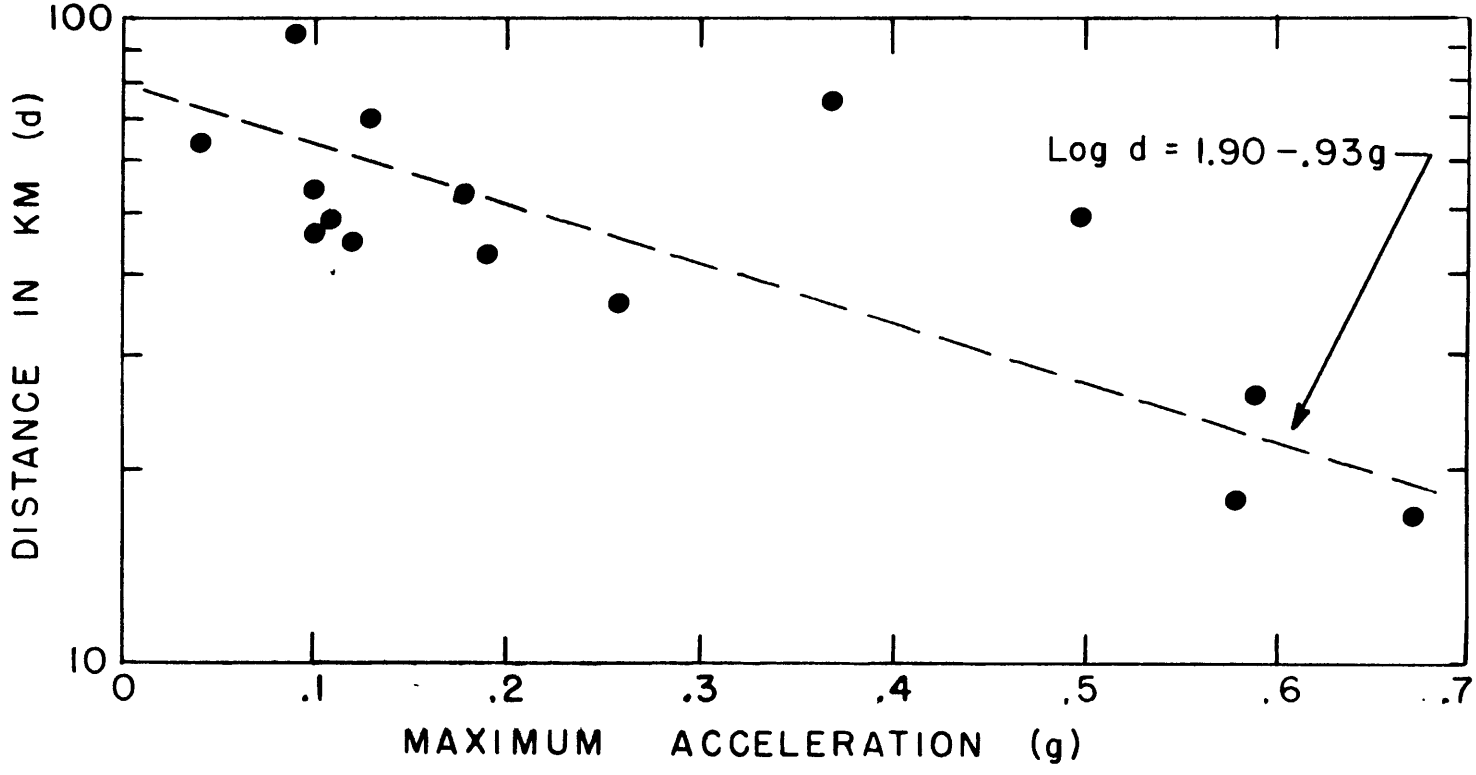

Figure 5. Maximum acceleration versus distance for the 6.6-magnitude Kaoiki earthquake from records of the U.S. Geological Survey, Hawaii network of strong-motion seismographs. The acceleration data was collected and provided by Arnold V. Acosta and Richard P. Maley of the U.S. Geological Survey.

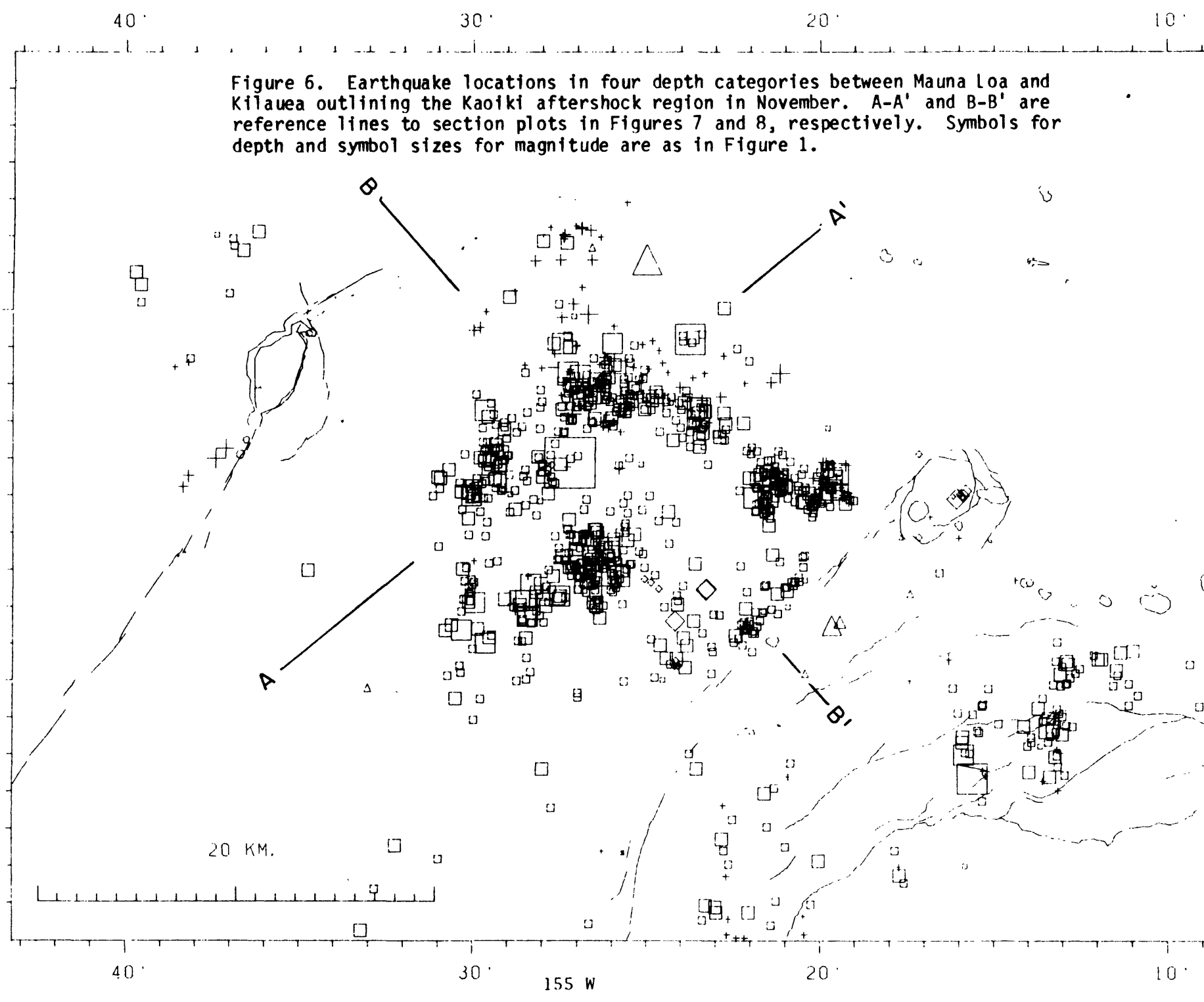

Figure 6. Earthquake locations in four depth categories between Mauna Loa and Kilauea outlining the Kaoiki aftershock region in November. A-A' and B-B' are reference lines to section plots in Figures 7 and 8, respectively. Symbols for depth and symbol sizes for magnitude are as in Figure 1.

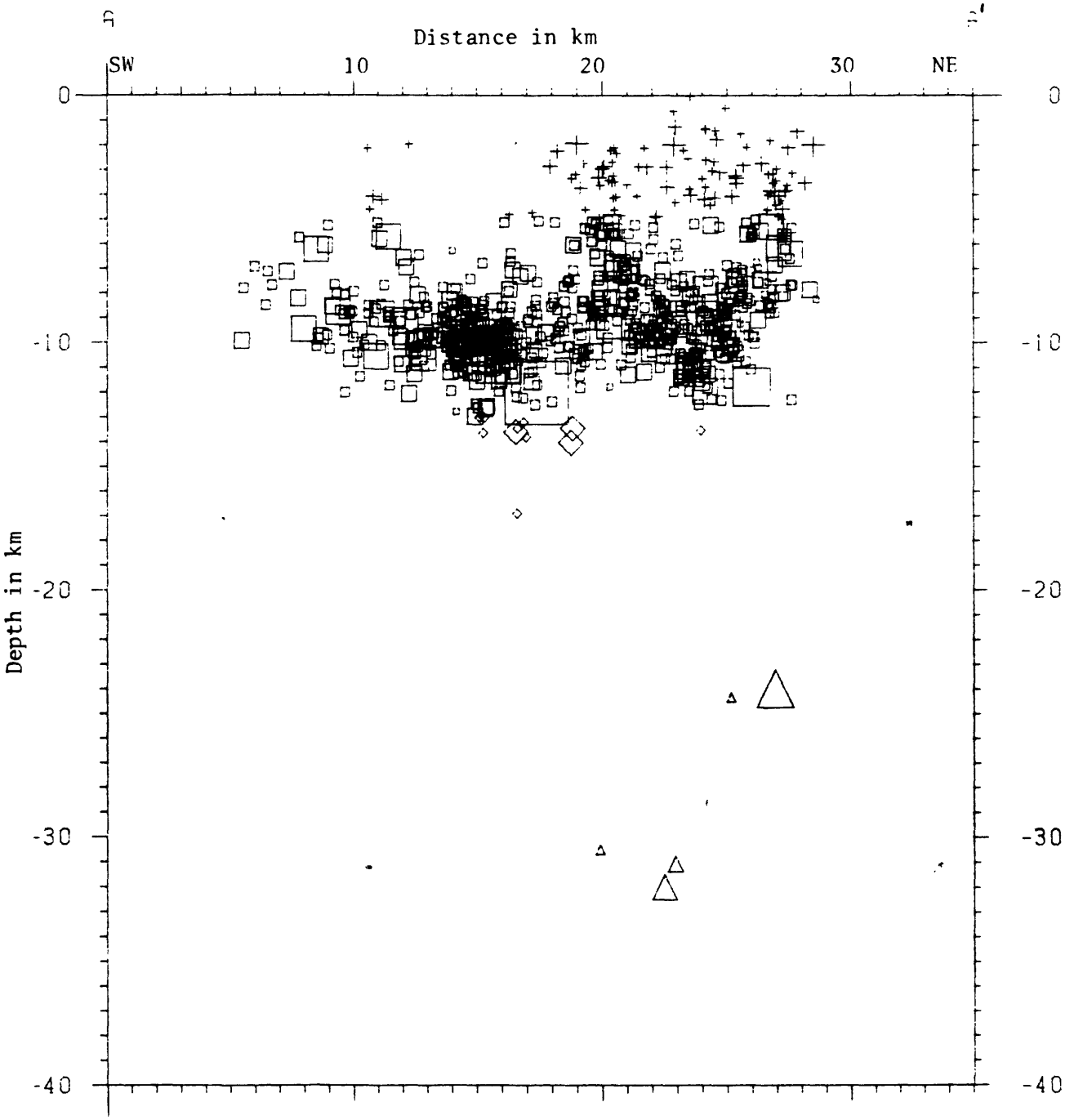

Figure 7. Kaoiki earthquakes in November viewed along a depth section normal to the plane centered on line A-A' in Figure 6.

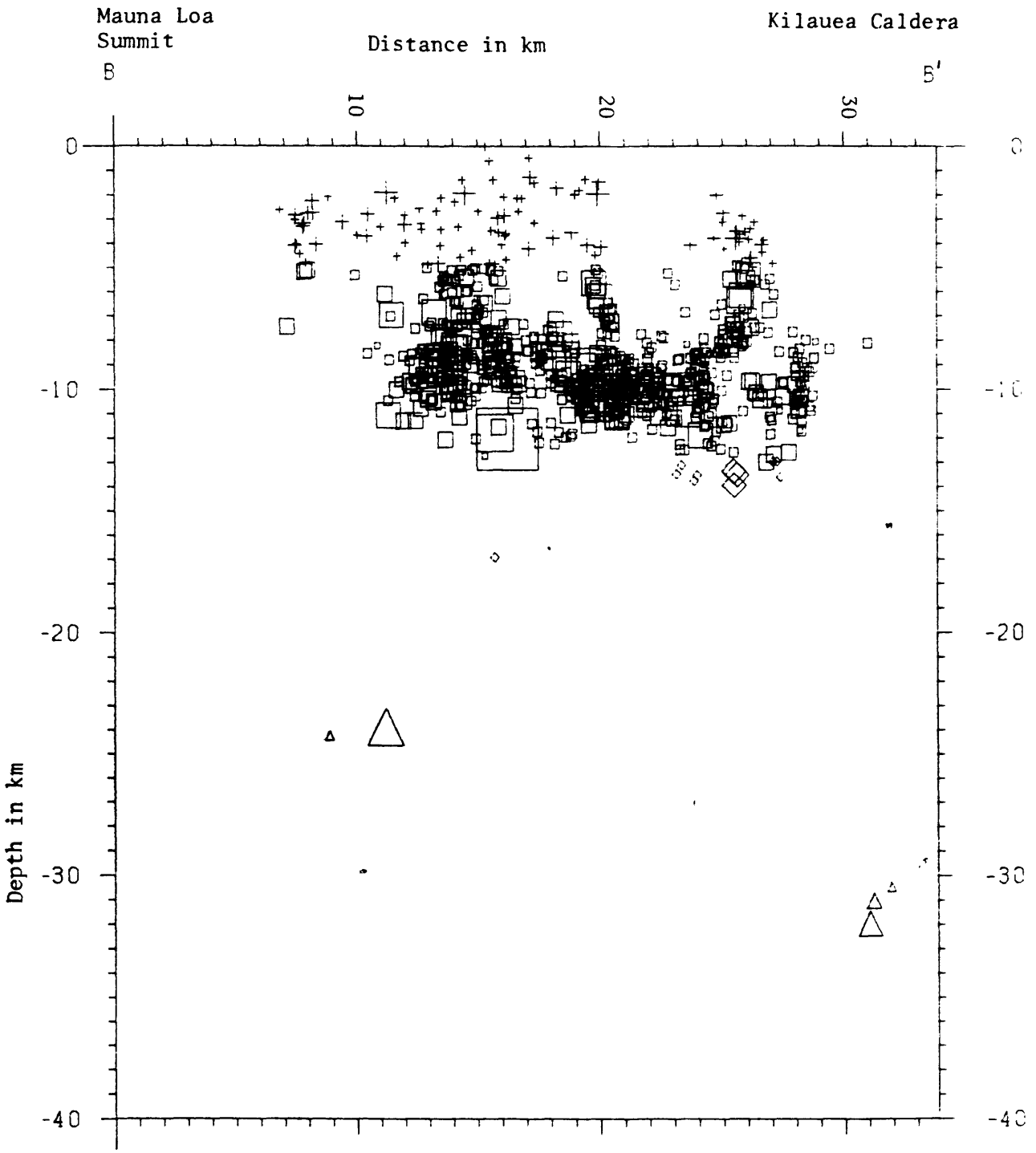

Figure 8. Kaoiki earthquakes in November viewed along a depth section normal to the plane centered on line B-B' in Figure 6.

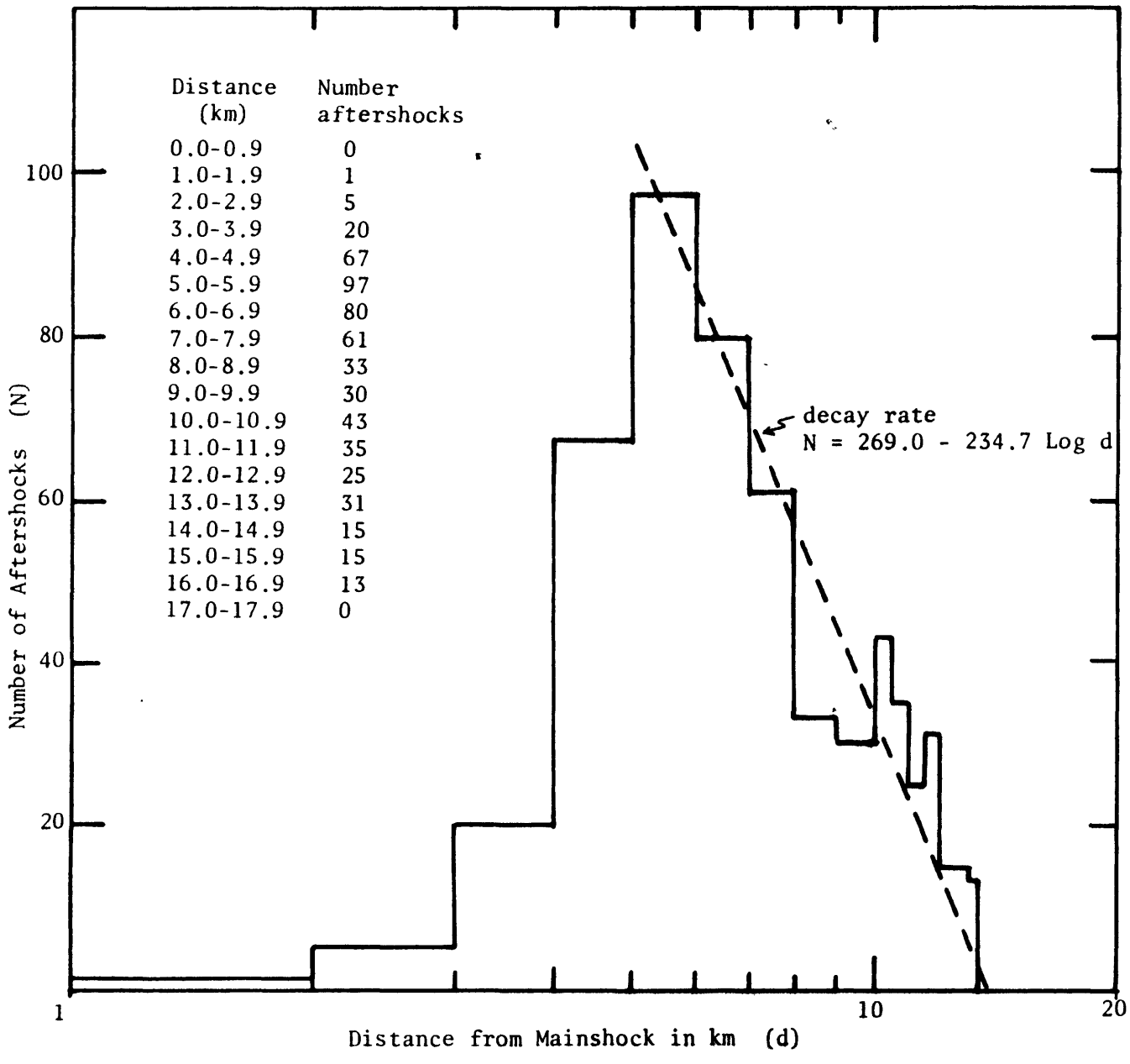

Figure 9. Number of aftershocks plotted as a function of distance from the principal shock on November 16. Included were aftershocks during the initial 8 days of activity and at $M \gtrsim 1.3$.

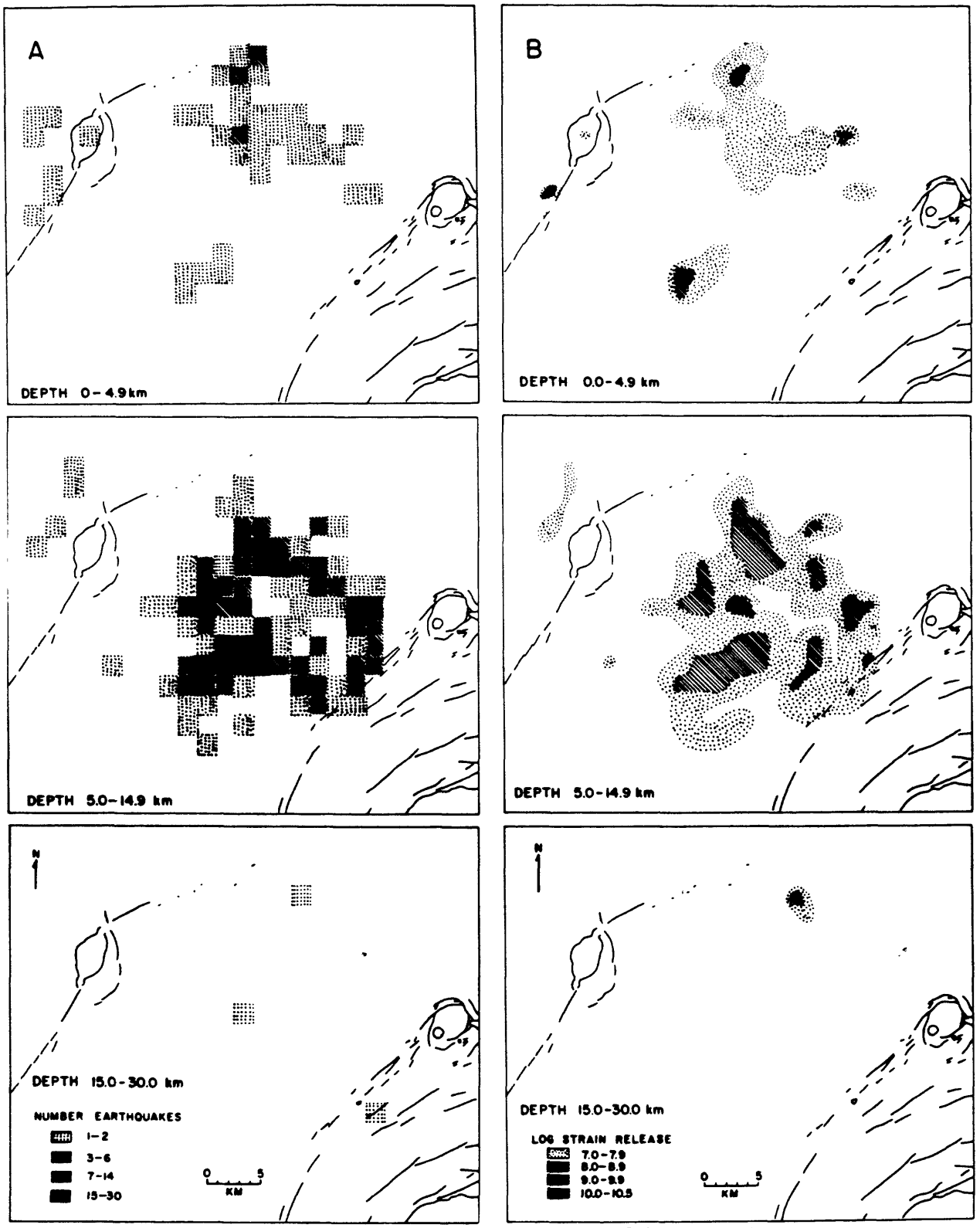

Figure 10. Earthquake density (column A, left) and seismic strain release (column B, right) maps in 3 depth categories for Kaoiki earthquakes during November 16 to December 31, 1983. Data included earthquakes of 2.0 magnitude or larger located within 19° 15' to 19° 35'N latitude and 155° 15' to 155° 40'W longitude.

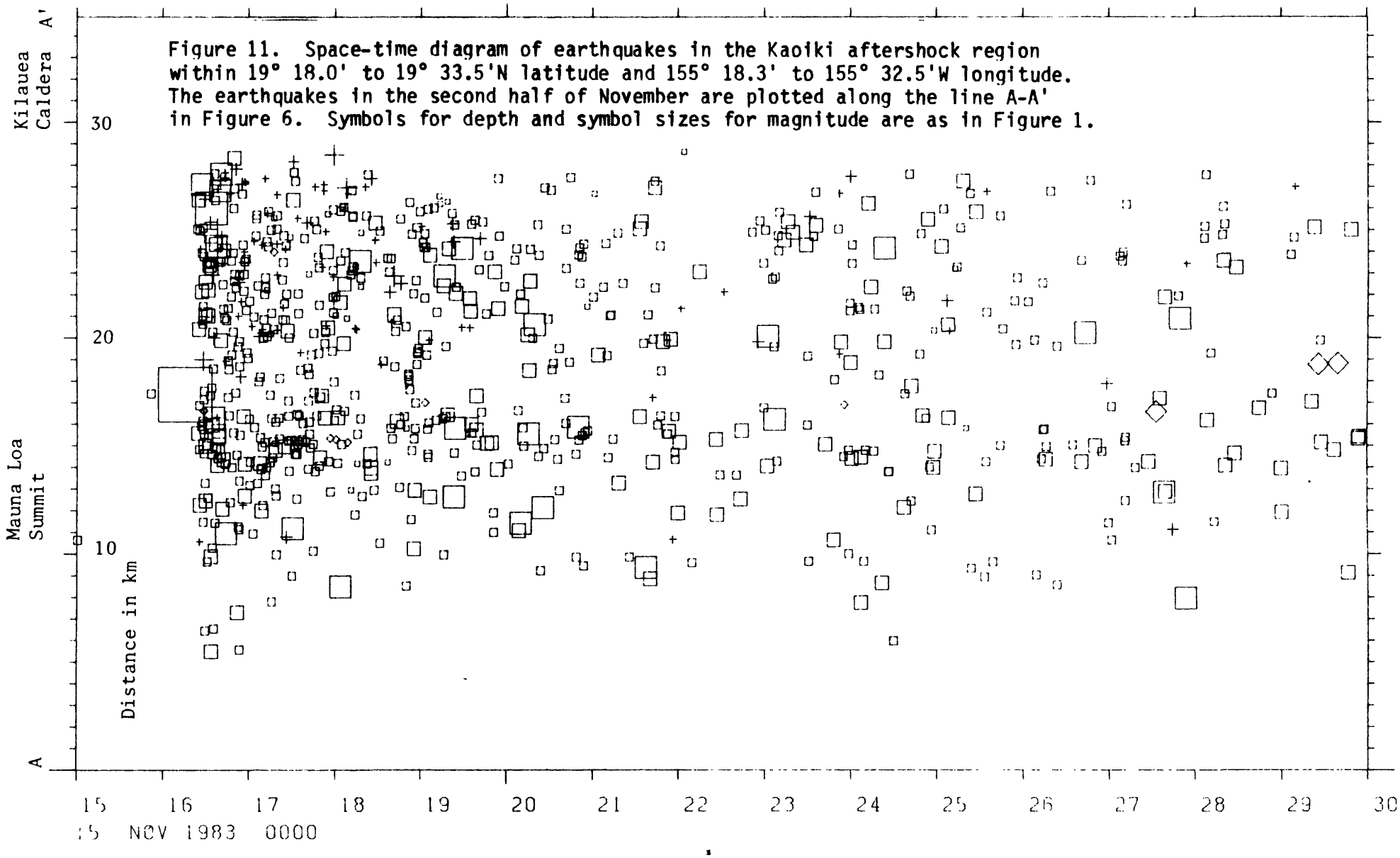

Figure 11. Space-time diagram of earthquakes in the Kaoiki aftershock region within 19° 18.0' to 19° 33.5'N latitude and 155° 18.3' to 155° 32.5'W longitude. The earthquakes in the second half of November are plotted along the line A-A' in Figure 6. Symbols for depth and symbol sizes for magnitude are as in Figure 1.

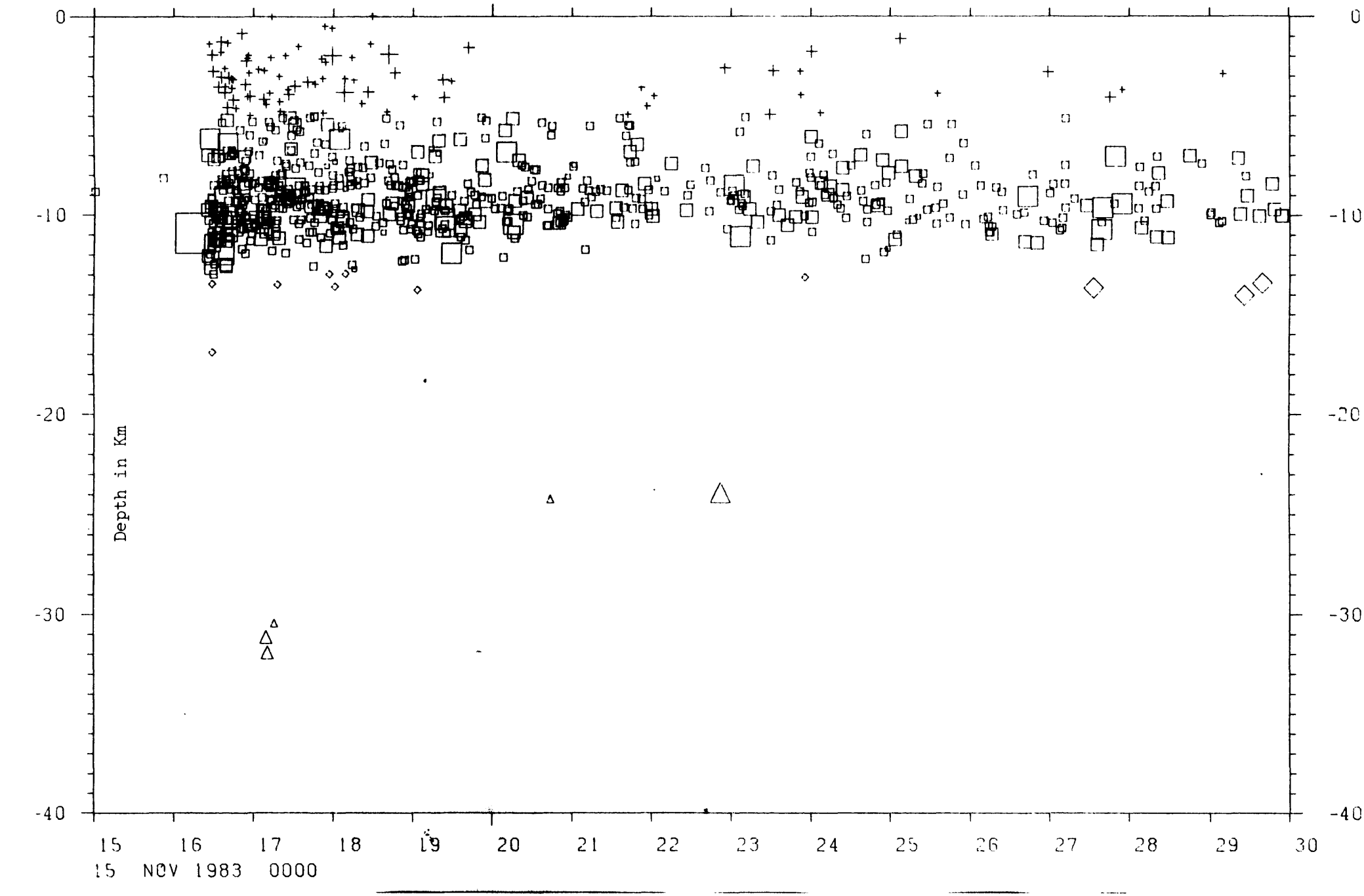

Figure 12. Depth-time plot of earthquakes in the Kaoiki aftershock region within the map coordinates 19° 18.0 to 19° 33.5'N latitude and 155° 18.3' to 155° 32.5'W longitude. Symbols for depth and symbol sizes for magnitude are as in Figure 1.

Figure 13. Magnitude-time plot of earthquakes in the Kaoiki aftershock region within the map coordinates 19° 18.0' to 19° 33.5'N latitude and 155° 18.3' to 155° 32.5'W longitude. Symbols for depth and symbol sizes for magnitude are as in Figure 1.

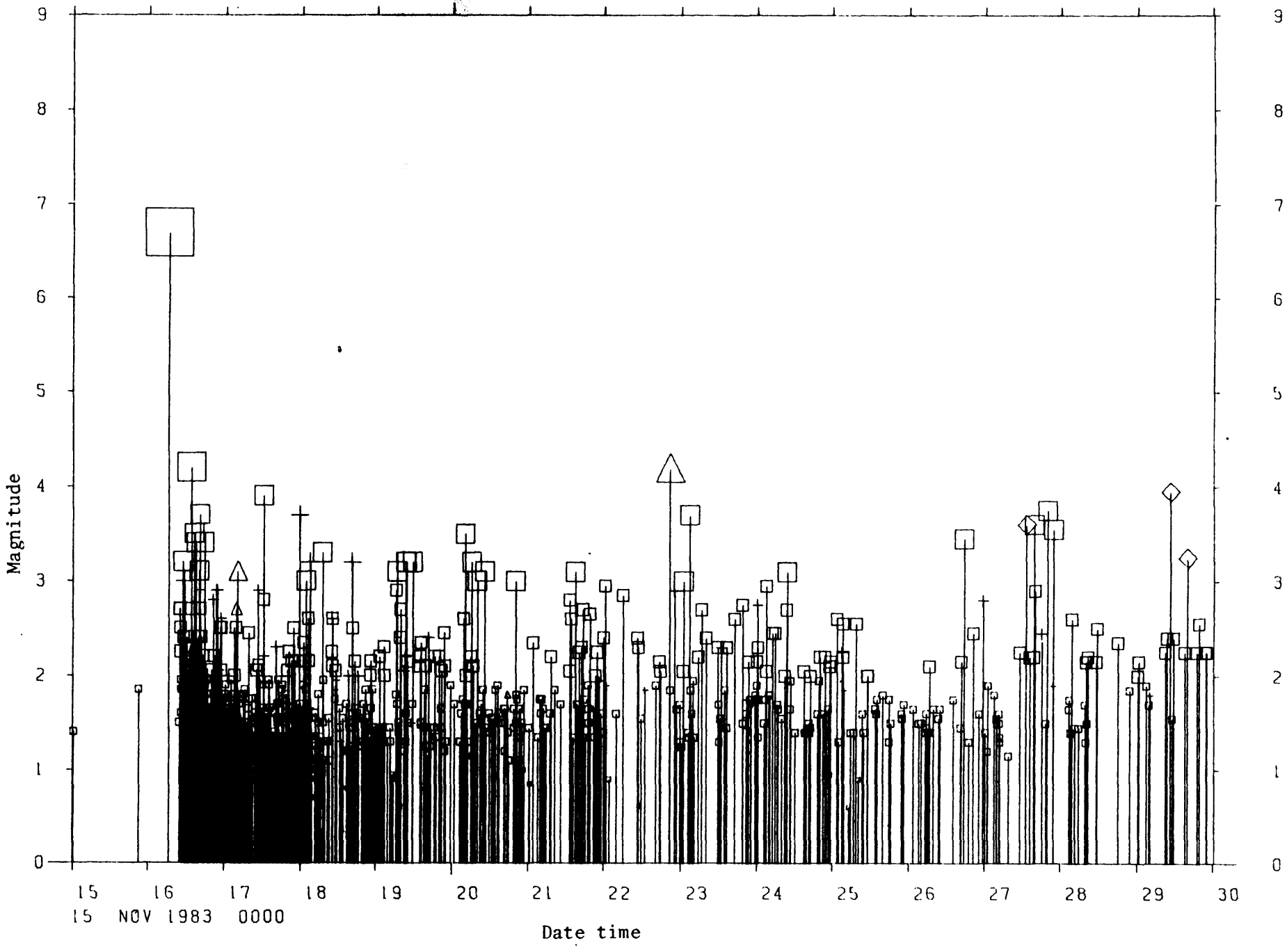

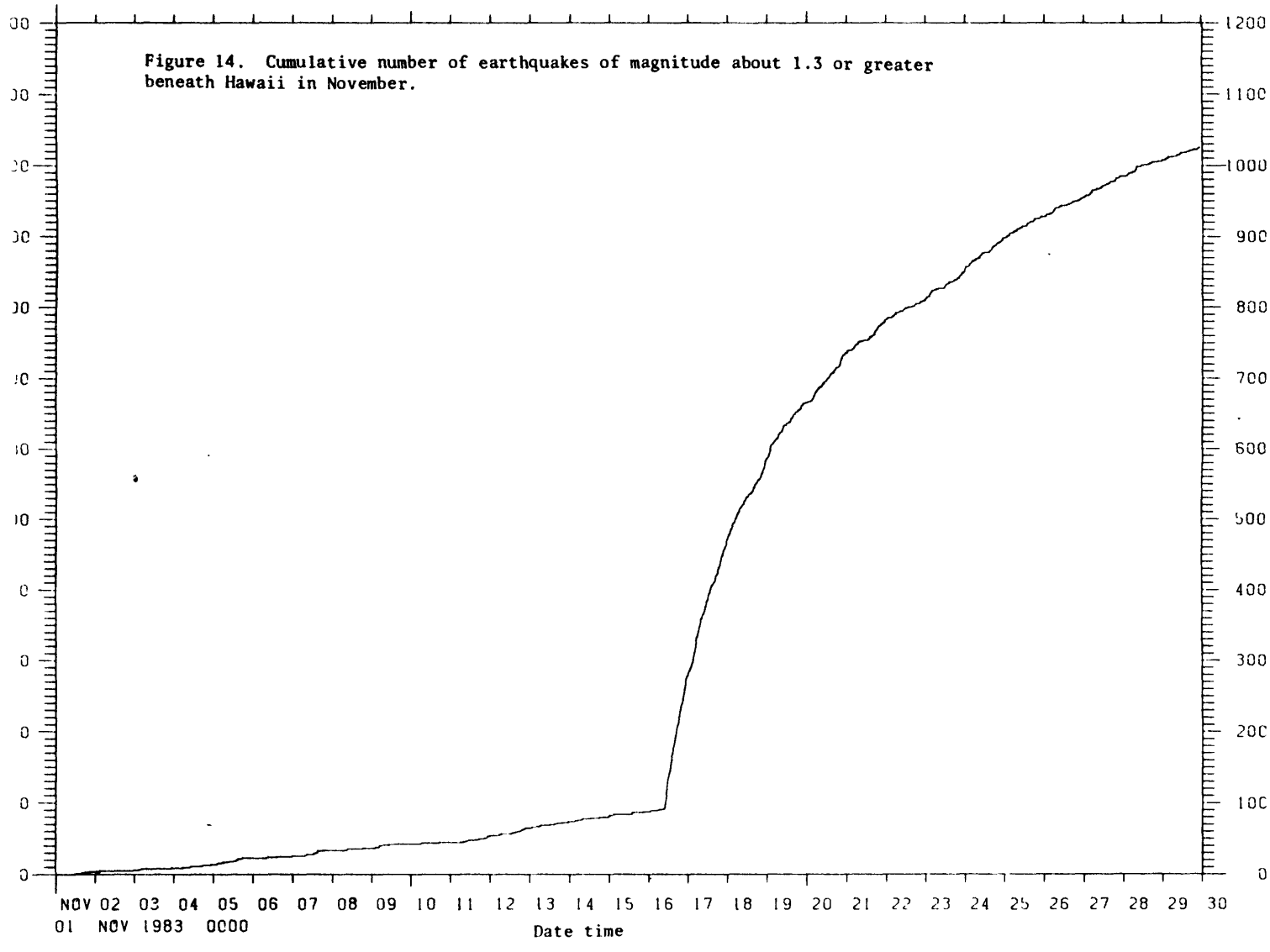

Figure 14. Cumulative number of earthquakes of magnitude about 1.3 or greater beneath Hawaii in November.

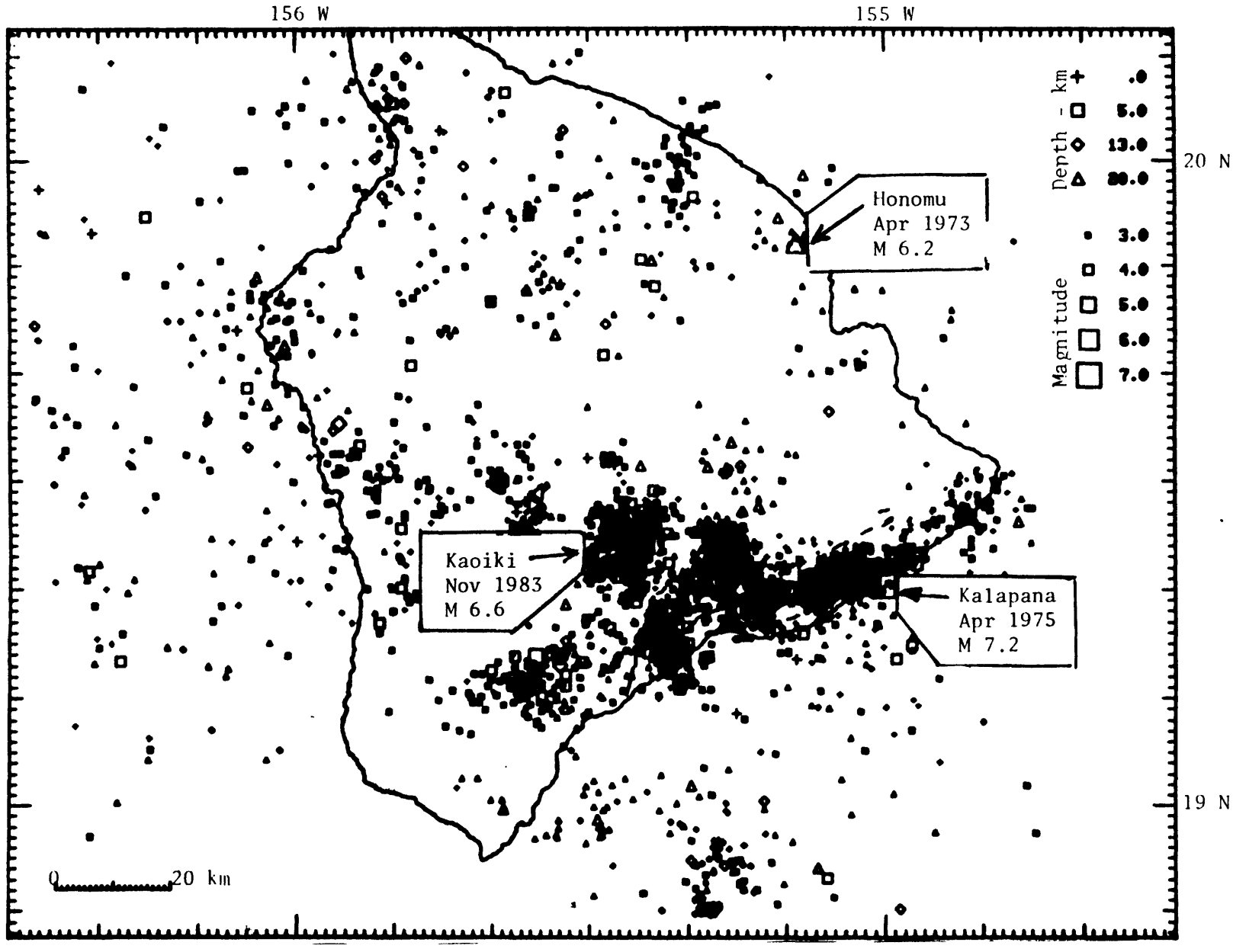

Figure 15. Location of earthquakes of magnitude 3.0 or larger in the region beneath the island of Hawaii from 1 January, 1962 to 30 November, 1983.

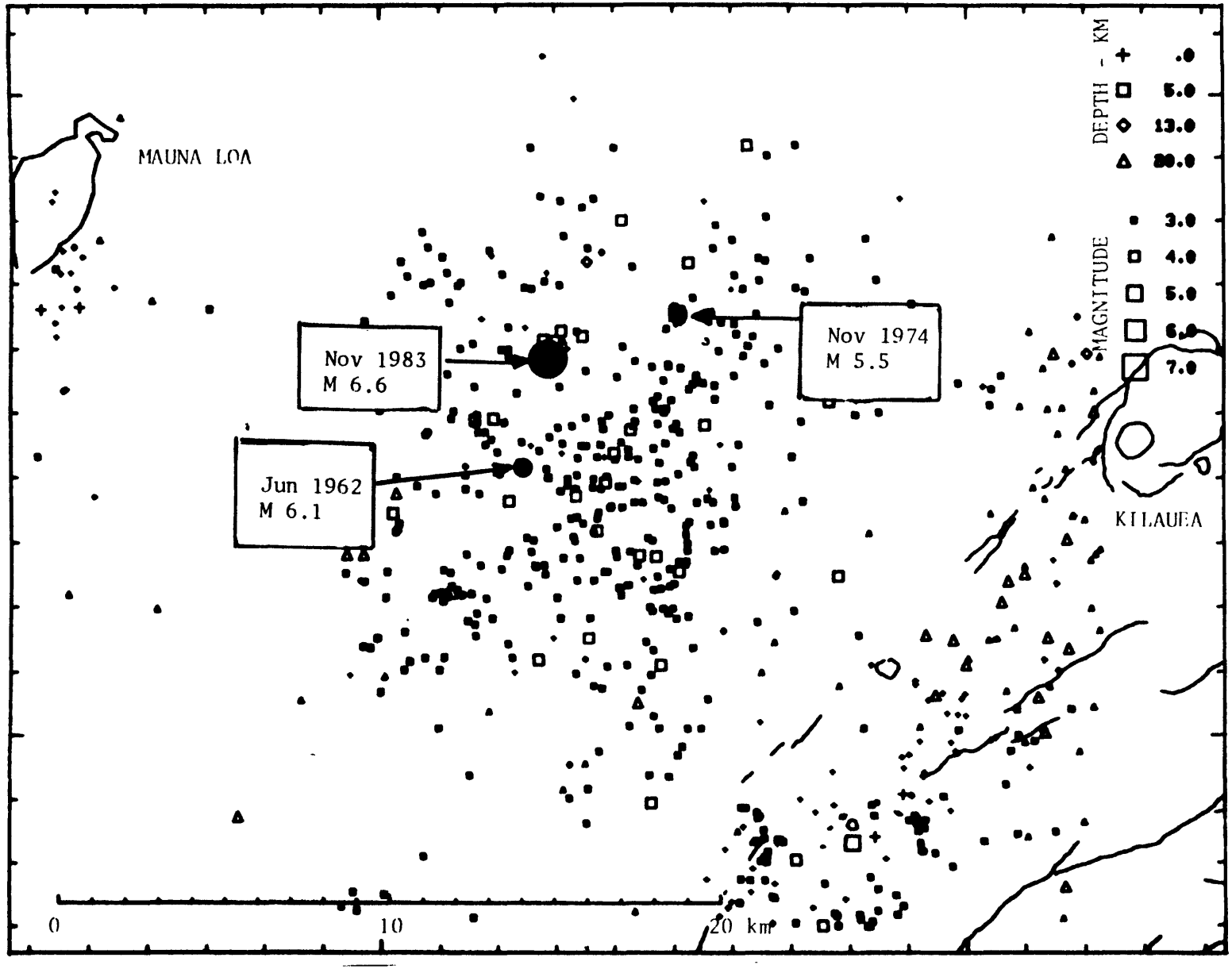

Figure 16, Location of earthquakes of magnitude 3.0 or larger in the Kaoiki region from 1 January, 1962 to 30 November, 1983.

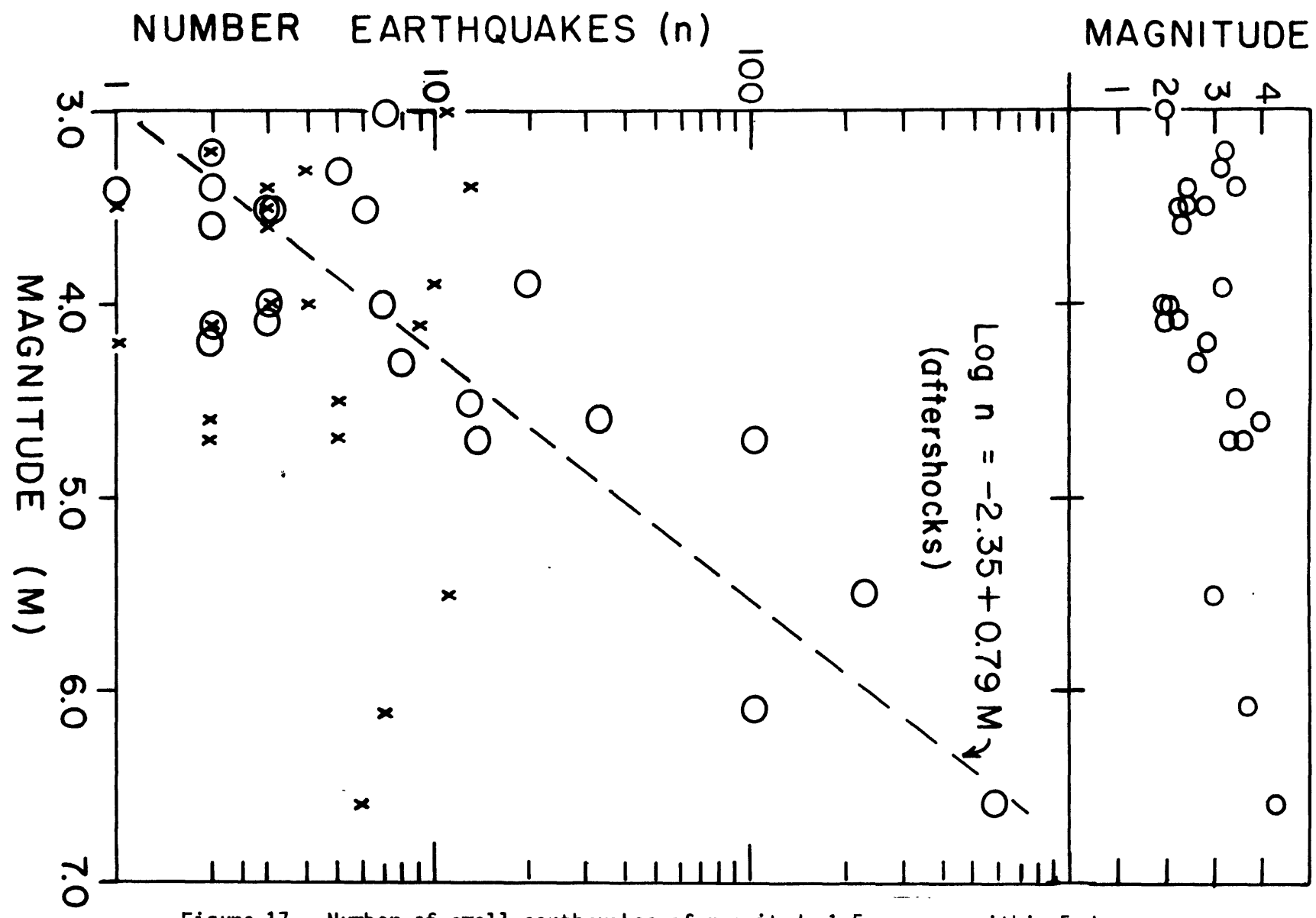

Figure 17. Number of small earthquakes of magnitude 1.5 or more within 5 days before (x), and within 5 days after (O) principal shocks of magnitude greater than 3.0 in the Kaoiki region. The dashed line is the averaged relation between the number of aftershocks and magnitude of the main shocks. Magnitude of the largest aftershock within 5 days following each of the respective principal shocks is shown in the plot to the right. Samples include Kaoiki earthquakes from 1962 to 1983.

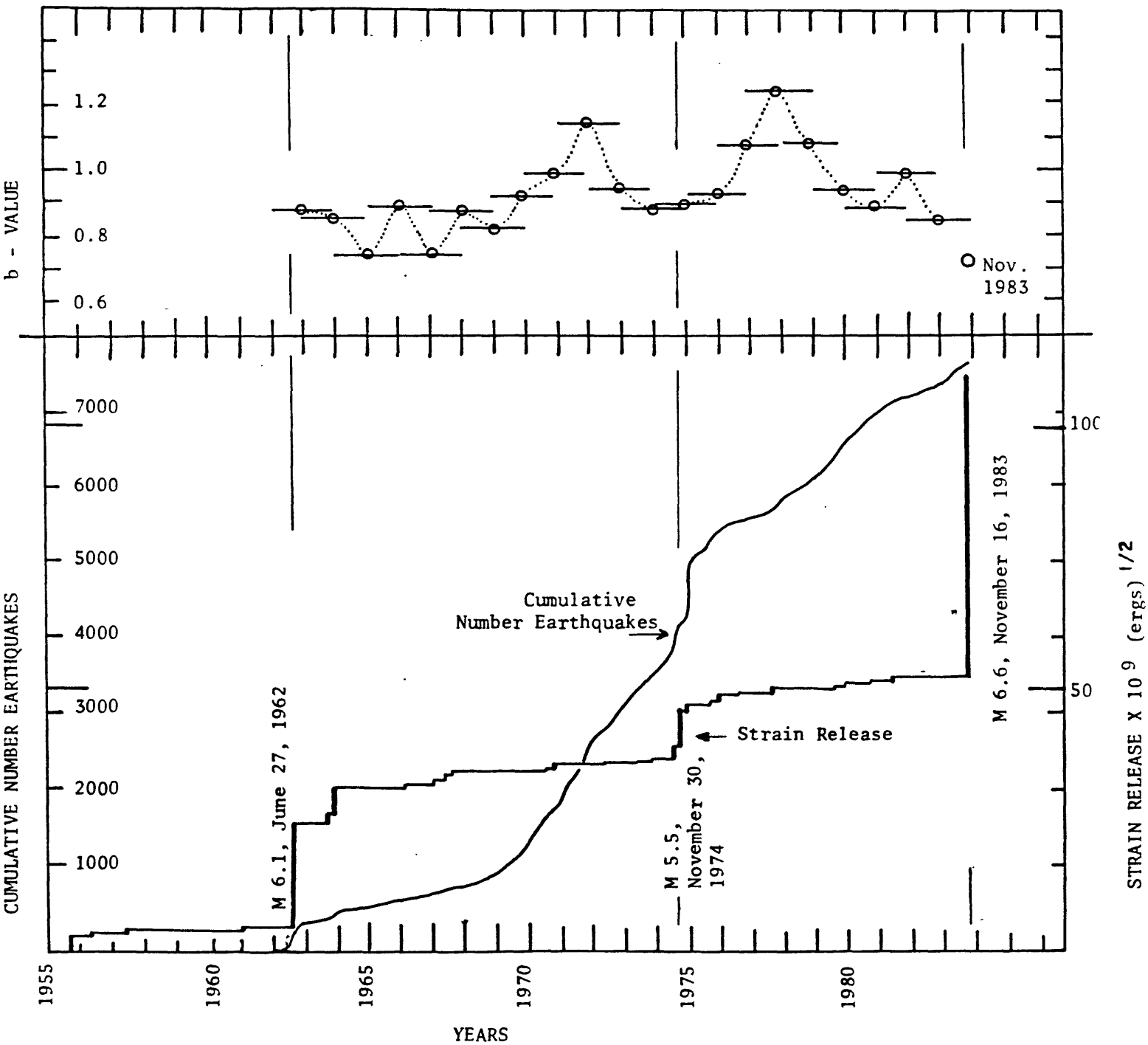

Figure 18. Cumulative number of Kaoiki earthquakes of magnitude about 1.5 or greater from January 1, 1962 to November 15, 1983, and cumulative strain release from earthquakes of magnitude 4.0 or greater from January 1, 1955 to November 30, 1983 (lower plot). Strain release was plotted as the square root of energy using Richter's energy-magnitude relation $\log E = 9.9 + 1.9M_l - 0.024M_l^2$. B-values, the magnitude-frequency parameter calculated from Kaoiki earthquakes of magnitude 1.5 or greater plotted as a function of time from January 1, 1962 to October 31, 1983 (higher plot). Samples were taken at 2-year increments with overlapping consecutive years. Value for November, 1983 was calculated and plotted separately.

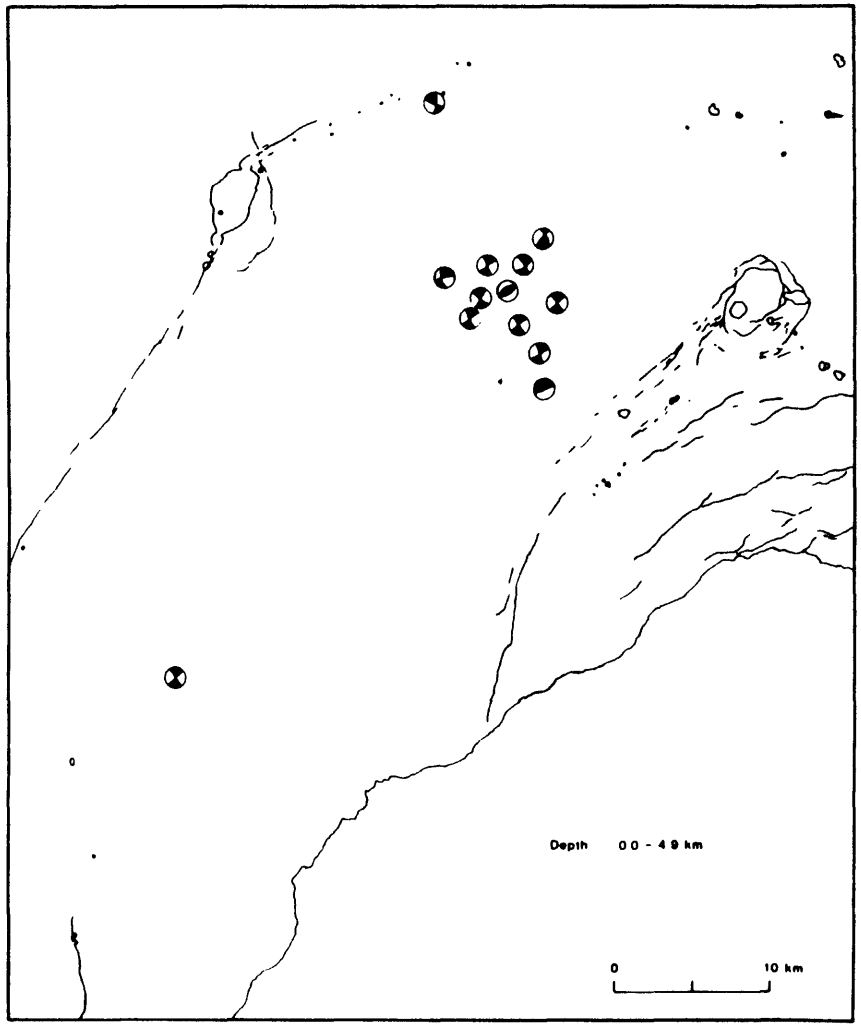

Figure 19a. Focal mechanisms from lower hemisphere projections for southeast Mauna Loa earthquakes 0-5 km in depth and from 1959 to 1982 in time (after Endo, 1984). Compressional field is black and dilatational area is white.

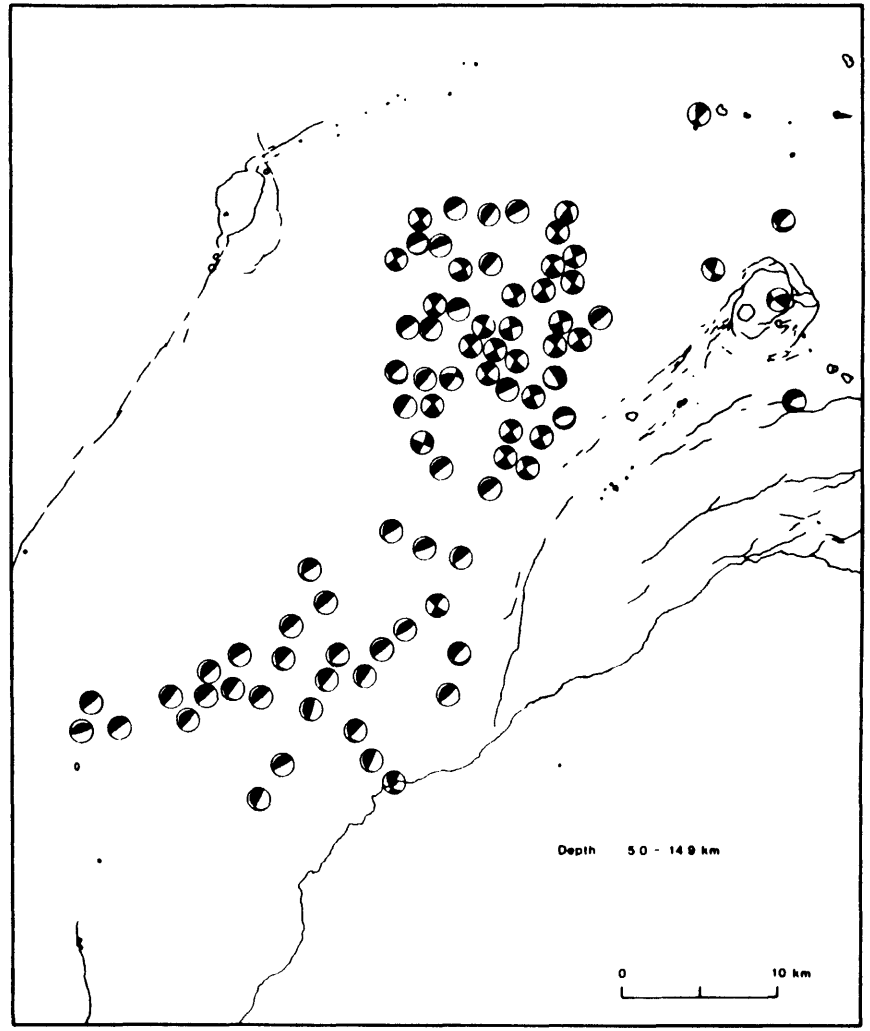

Figure 19b. Focal mechanism from lower hemisphere projections for Mauna Loa earthquakes 5 to 15 km in depth and from 1959 to 1982 in time (after Endo, 1984). Compressional field is black and dilatational area is white.

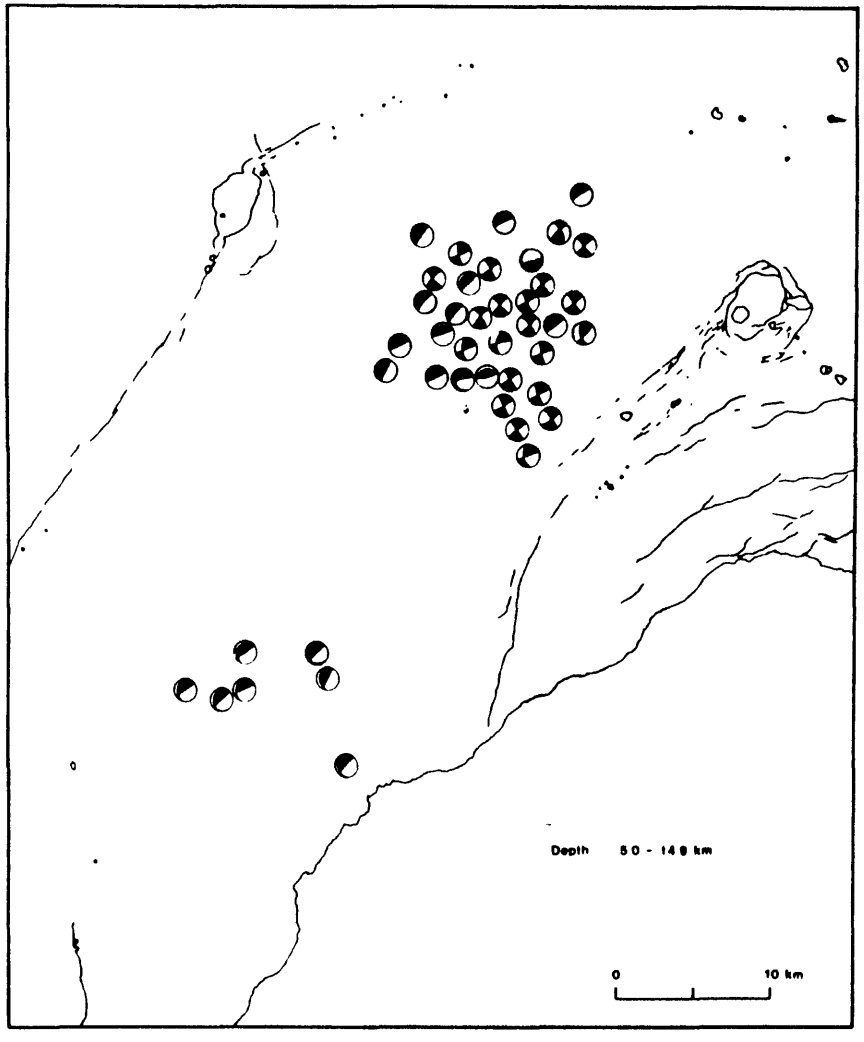

Figure 19c. Focal mechanism from lower hemisphere projections for Mauna Loa earthquakes 5 to 15 km in depth and from 1959 to 1982 in time (after Endo, 1984). Compressional field is black and dilatational area is white.

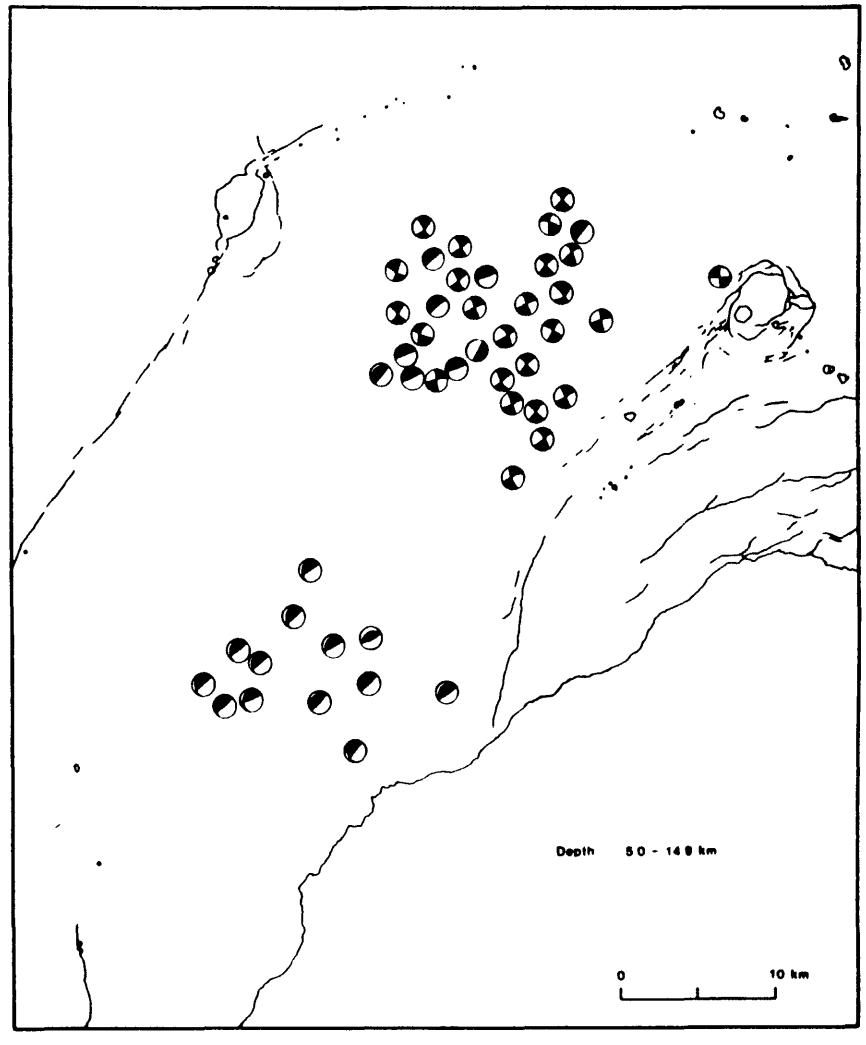

Figure 19d. Focal mechanism from lower hemisphere projections for Mauna Loa earthquakes 5 to 15 km in depth and from 1959 to 1982 in time (after Endo, 1984). Compressional field is black and dilatational area is white.

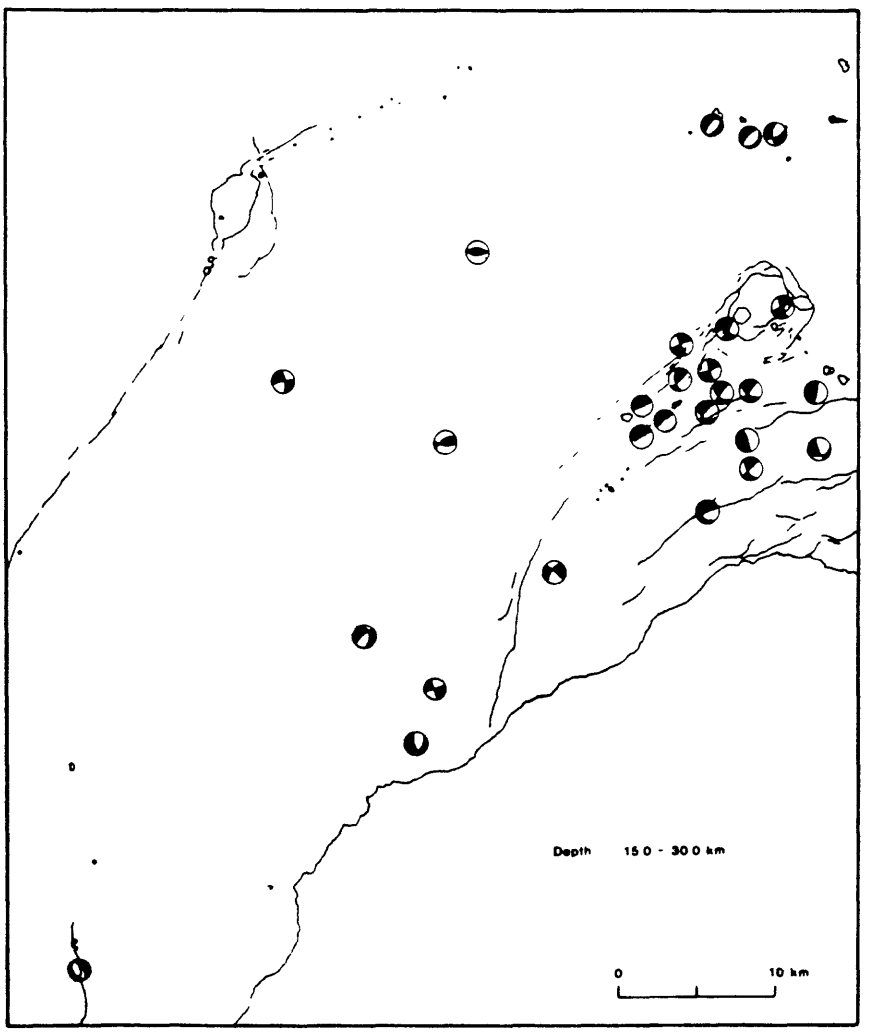

Figure 19e. Focal mechanism from lower hemisphere projections for Mauna Loa earthquakes 15 to 30 km in depth and from 1959 to 1982 in time (after Endo, 1984). Compressional field is black and dilatational area is white.

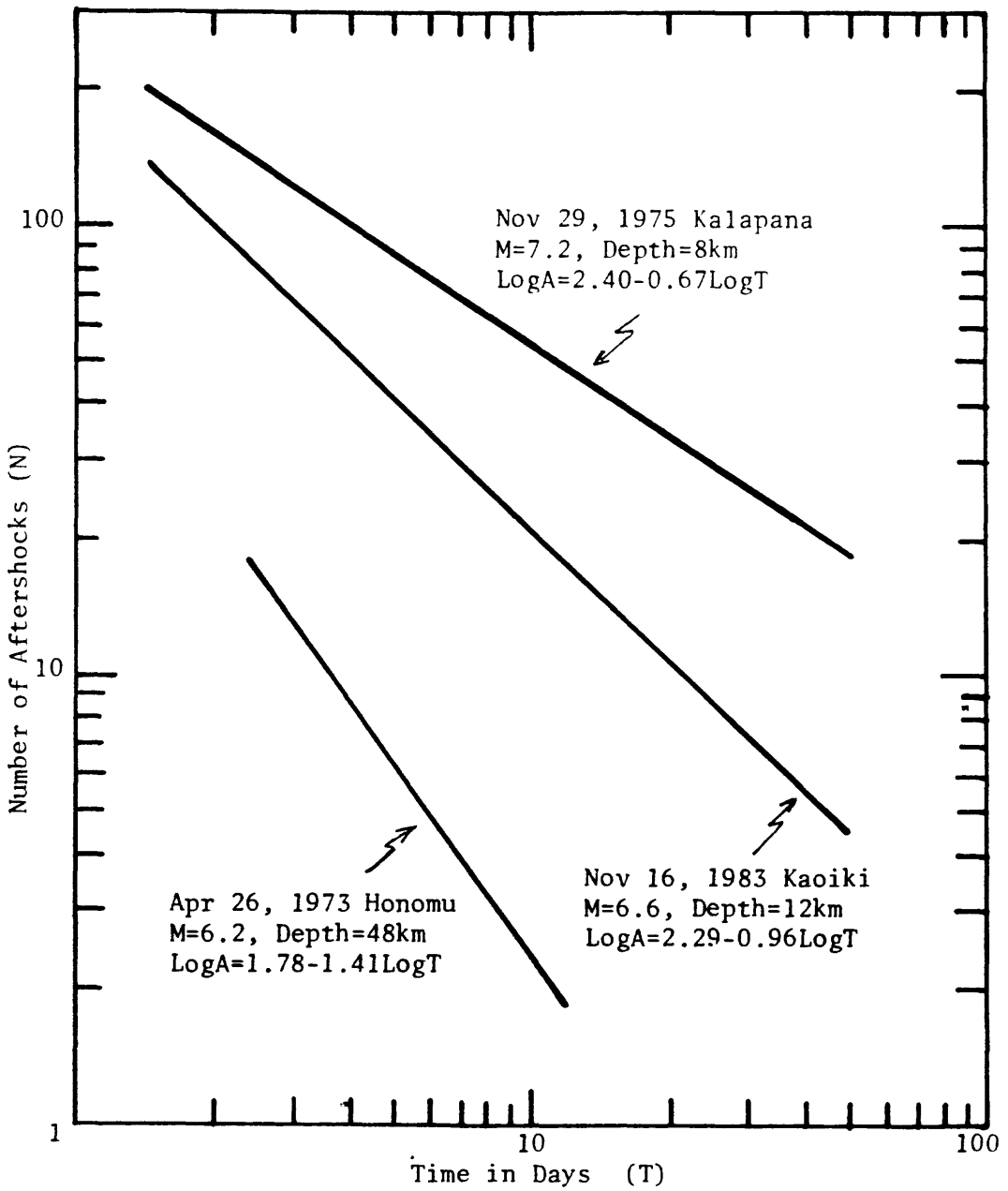

Figure 20. Aftershock decay rate for 3 large earthquakes in Hawaii. The rates were approximated from the daily number of magnitude 1.5 or larger aftershocks plotted logrithmically as a function of time for the initial 50 days of activity.

Figure A1. Digitized seismogram of a 1.6-magnitude and 9.4 km deep Kaoiki earthquake on March 20, 1980 at station AIN. Station-to-epicenter distance was 3 km. The dots placed at 02:12:11 mark the calculated origin time of the earthquake to the nearest second. The portion of the seismogram extending from 6 to 17 seconds after origintime as indicated by the horizontal arrow was used to determine the signal decay rate.

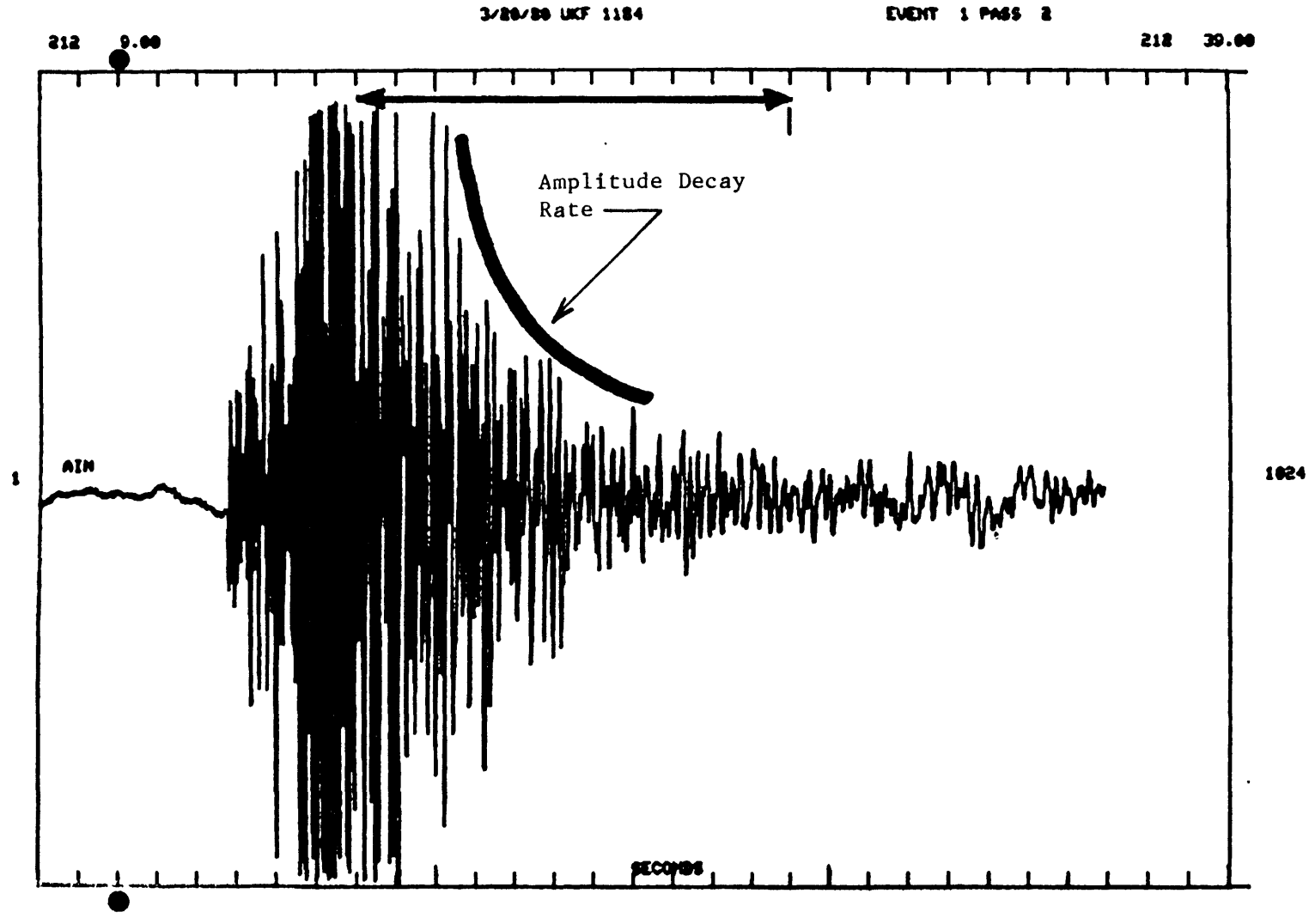

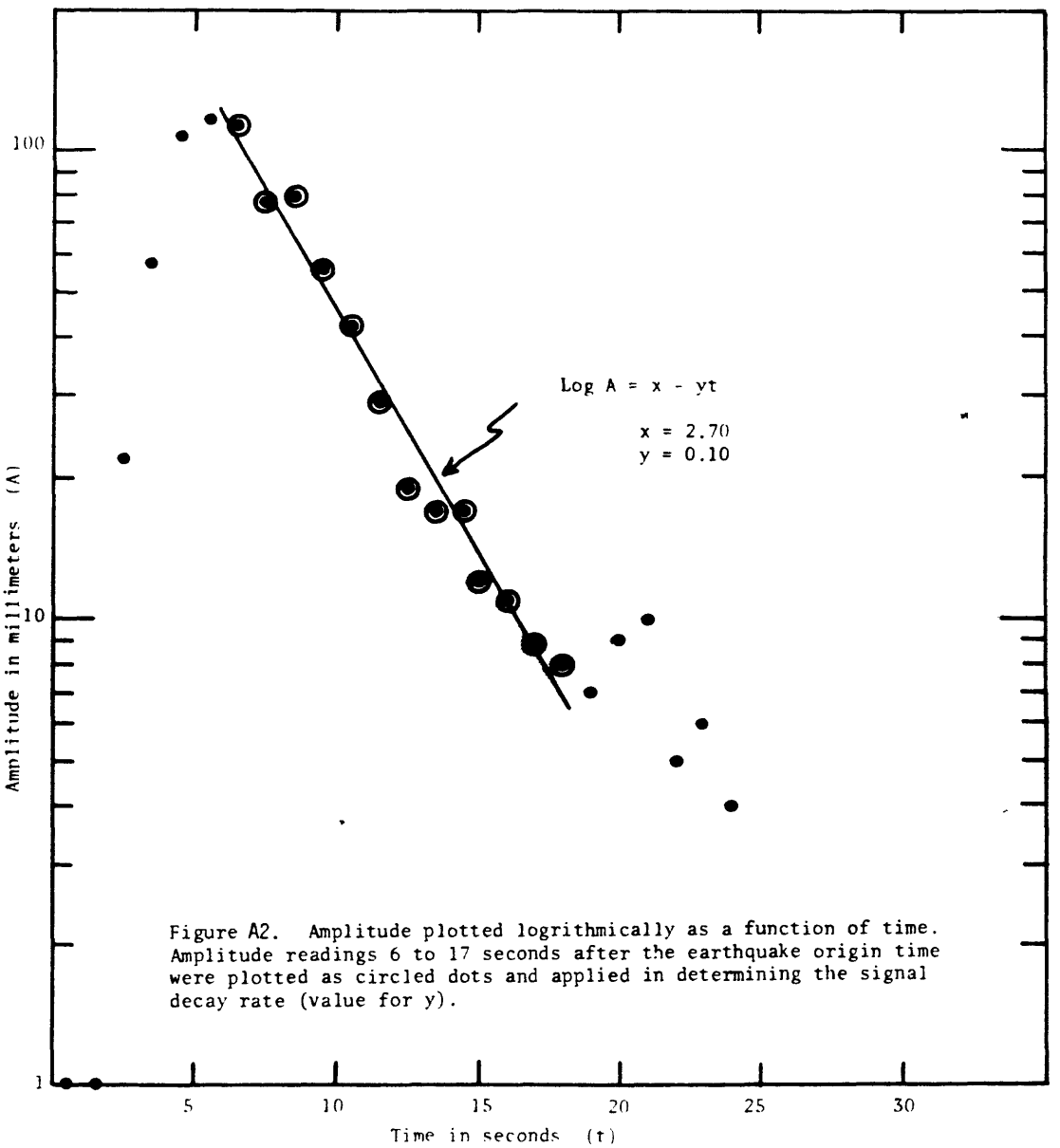

Figure A2. Amplitude plotted logrithmically as a function of time. Amplitude readings 6 to 17 seconds after the earthquake origin time were plotted as circled dots and applied in determining the signal decay rate (value for y).

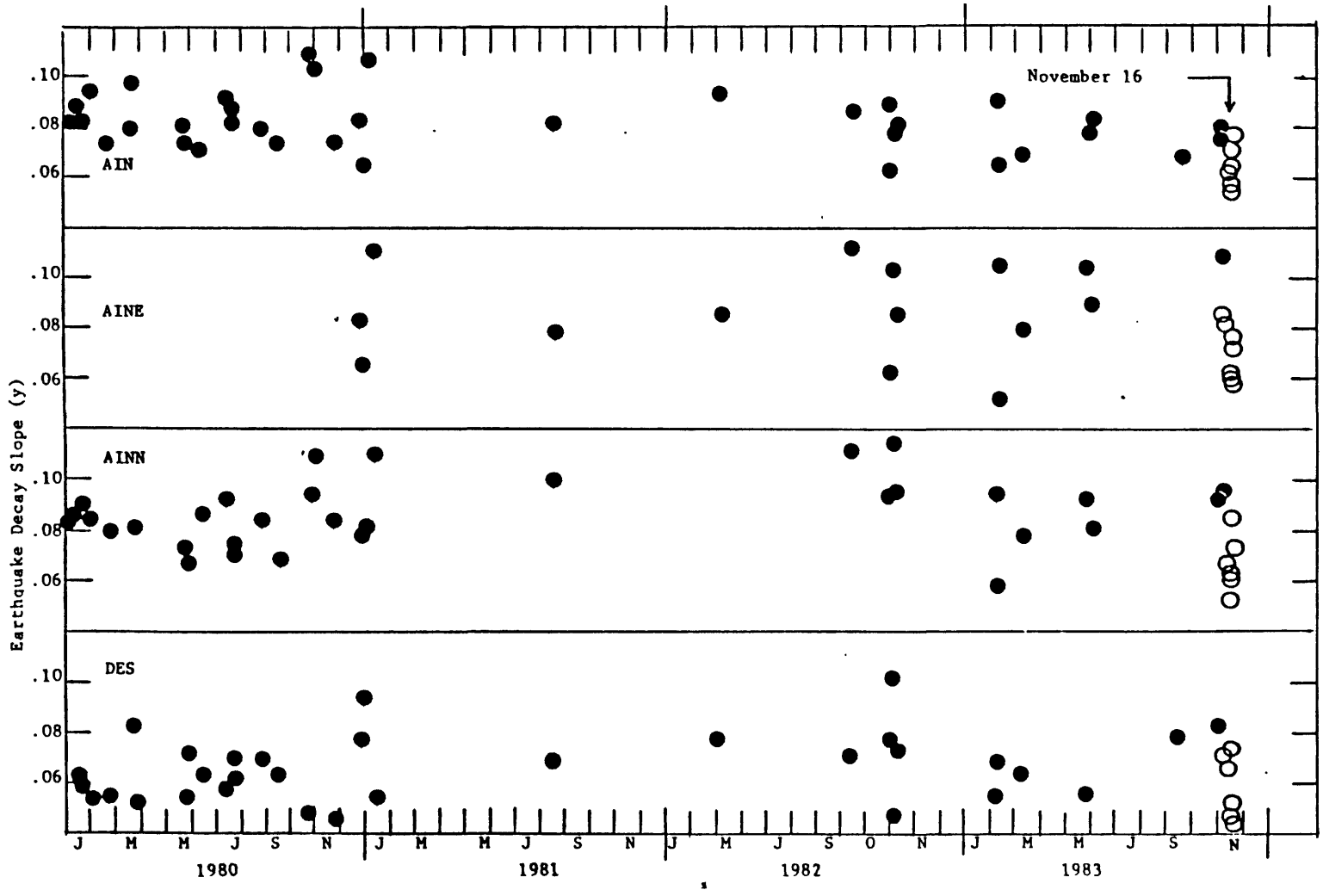

Figure A3. Coda decay slope as a function of time for selected small Kaoiki earthquakes before and after the major Kaoiki earthquake on November 16.

Table 1. Seismic parameters of damaging earthquakes and their aftershocks in Hawaii from 1962 to 1983.

Date and Location of Earthquake	Magnitude	Energy Release (ergs x 10^{20})	Maximum MM Intensity and Location	Damage $ Millions	Depth KM	Focal Mechanism	Aftershock zone volume (lxwxh)	Number of aftershocks $M \geq 1.5$ and Largest aftershock initial 5 days	Duration in Years Aftershock Activity $M \geq 0.1$
June 27, 1962 Kaoiki	6.1	4	VI Volcano, Kapapala	1.0 (?)	8	strike-slip	(10x10x10) 1000 km^3	103; M 3.7	0.1
April 26, 1973 Honomu	6.2	6	VII Hilo, Hamakua	5.6	48	strike-slip	(20x10x15) 3000 km^3	105; M 3.4	0.1
November 29, 1975 Kalapana	7.2	217	VIII Hilo, Puna Volcano	4.1	8	Low-angle thrust	(50x10x10) 5000 km^3	730; M 4.3	3.0
November 16, 1983 Kaoiki	6.6	26	VIII-IX Volcano, Kapapala, Hilo	7.0 (?)	12	strike-slip	(20x20x10) 4000 km^3	580; M 4.3	0.3